Mechanism exploration of Wang's empirical formula on hepatoprotection in MAFLD via metabolomics and microbiomics

Suhong Chen[1,3,4,a], Jiahui Huang[1,4,b], Chengliang Zhou[1,4,c], Simei Dong[1,4,d], Yibin Wang[1,4,e], Ning Wang[1,4,f], Jiujie Jia[1,4,g], Chuanjie Zhou[1,4,h], Xinglishang He[1,3,4,i], Bo Li[1,4,j], Kungen Wang[2,5,k], Yihui Zhi[2,5,m], Guiyuan Lv[3,n], Shuhua Shen[2,5,*]

[1]Collaborative Innovation Center of Yangtze River Delta Region Green Pharmaceuticals, Zhejiang University of Technology, Hangzhou, Zhejiang, 310014, China
[2]The First Affiliated Hospital of Zhejiang Chinese Medical University, Hangzhou, Zhejiang, 310006, China
[3]College of Pharmaceutical Science, Zhejiang Chinese Medical University, Hangzhou, Zhejiang, 310053, China
[4]Zhejiang Provincial Key Laboratory of TCM for Innovative R&D and Digital Intelligent Manufacturing of TCM Great Health Products, Huzhou, Zhejiang, 313200, China
[5]Kungen Wang National Famous Chinese Medicine Doctor Studio, Hangzhou, Zhejiang, 310006, China

[a]Email：chensuhong@aliyun.com
[b]Email：cjhcf0706@foxmail.com
[c]Email：211122230016@zjut.edu.cn
[d]Email：dongsimei2001@163.com
[e]Email：18358537898@163.com
[f]Email：201805150210@zjut.edu.cn
[g]Email：2278510288@qq.com
[h]Email：zhoucj99@foxmail.com
[i]Email：837479921@qq.com
[j]Email：boli19861023@163.com
[k]Email：wkg1220@163.com
[m]Email：medcat4@163.com
[n]Email：zjtcmLgy@163.com
[*]Corresponding author Email：linba0358@163.com

Funding：This study was supported by National Natural Science Foundation of China (No. 81503527),National Natural Science Foundation of China (No. 82274134),National Key Research and Development Plan (No. 2017YFC1702200),National Key Research and Development Plan (No. 2017YFC1702202),Key Research and Development Program of Zhejiang Province (No. 2020C04020),Science and Technology Department of the State Administration of Traditional

Chinese Medicine Zhejiang Province Joint Project (No. GZY-ZJ-KJ-24068)

These authors contributed equally.

Suhong Chen ,Jiahui Huang ,Chengliang Zhou ,Simei Dong (Co-first author)

Highlights

1. WSF improved MAFLD in a dose-dependent manner.
2. WSF regulated BA metabolism by increasing the abundance of *Lactobacillus*.
3. WSF modulated FXR pathways, alleviated hepatic lipid deposition.

Abstract

Background: Metabolic-dysfunction associated fatty liver disease (MAFLD) is the most prevalent liver disorder globally. Wang's empirical formula (WSF), a Traditional Chinese Medicine preparation, was developed by Prof. Kungen Wang. Although it has been used clinically for years, the exact therapeutic mechanism by which WSF addresses MAFLD is not fully understood.

Methods: A high-sugar and high-fat diet (HSHFD) was used to establish MAFLD model rats to observe the effects of WSF on physical signs, lipid metabolism, glucose metabolism and liver histopathology. The mechanism of WSF based on the modulation of gut flora and bile acid (BA) metabolism for the treatment of MAFLD will then be explored using targeted metabolomics, gut flora, Western blot, and PCR.

Results： WSF19.8 g/kg showed a more comprehensive effect. It reduced body weight, serum TC, TG, LDL-c, and NEFA, lowered blood glucose, attenuated insulin resistance, and reduced visceral fat accumulation, hepatic steatosis, and inflammation in MAFLD model rats. WSF reduced BA pools, increased BA excretion, improved hepatic BA profile, and increased CDCA group in MAFLD rats. WSF increased the relative abundance of *Lactobacillus* and *norank_f__Eubacterium_coprostanoligenes_group* at the genus level, and decreased the relative abundance of *Blautia*. WSF inhibited the expression of the intestinal FXR-FGF15-FGFR4 pathway and ASBT expression, activated the hepatic FXR-SHP pathway, and consequently up-regulated hepatic CYP27A1, BSEP and PPAR-α expression, and inhibited the expression of SREBP-1c, SREBP-2, ACC, and SCD-1 (**Figure 1**).

Conclusions: WSF has an ameliorative effect on MAFLD. Its mechanism may be related to regulating gut flora and BA metabolism, targeting the FXR-related pathway, promoting the conversion of hepatic cholesterol to BAs, facilitating BA efflux and lipid β-oxidation, and inhibiting de novo lipogenesis (DNL).

Keywords: Wang's empirical formula, FXR, gut flora, bile acid, MAFLD

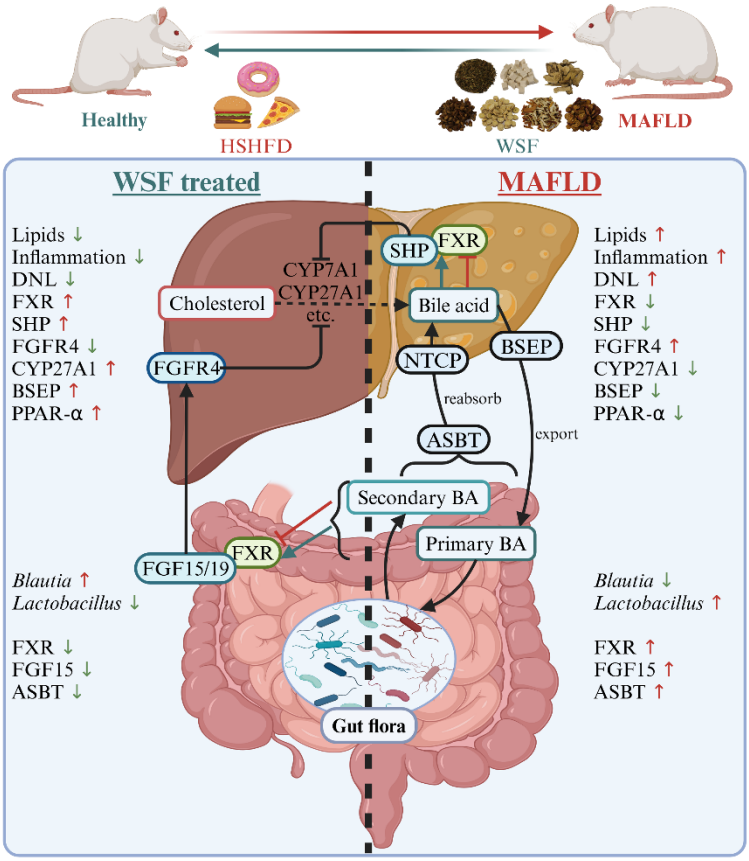

Figure 1 Graphic abstract (Created in BioRender.com)

1. Introduction

As societies have developed, per capita calorie intake has increased dramatically, and the proportion of calories provided by fat and carbohydrates has increased, leading to a gradual increase in the prevalence of MAFLD caused by over-nutrition[1]. The aggregate prevalence of MAFLD among Chinese adults reaches 29.8%, positioning China as the nation with the greatest prevalence, morbidity, and annual mortality from MAFLD-related diseases in Asia. Fatty liver can progress to steatohepatitis, fatty liver fibrosis, and in severe cases, can even lead to liver cancer. It is essential to conduct comprehensive research into the pathogenesis, prevention and treatment of MAFLD. Currently, Rezdiffra is the only drug approved by the FDA to treat non-alcoholic steatohepatitis, and it must be used in combination with exercise and dietary changes.

Traditional Chinese Medicine (TCM) has clear advantages and characteristics in preventing and treating metabolic diseases such as MAFLD. According to the "*Expert Consensus on Traditional Chinese Medicine Diagnosis and Treatment of Non-alcoholic Fatty Liver Disease (2023)*", the fundamental pathogenesis of fatty liver disease lies in the dysfunction of the spleen and stomach's transportation and transformation, with the pathological feature primarily dominated by phlegm and dampness[2]. WSF was developed for the remedy of metabolic diseases by Prof.

Kungen Wang, the first national famous doctor of TCM and national academic leader of "spleen and stomach disease of TCM". WSF is composed of *Gynostemmae Herba* (Jiaogulan), *Astragali Radix* (Huangqi), *Crataegi Fructus* (Shanzha), *Salviae Miltiorrhizae Radix et Rhizoma* (Danshen), *Poria* (Fuling), *Atractylodis Macrocephalae Rhizoma* (Baizhu), and *Citri Reticulatae Pericarpium* (Chenpi). Meanwhile, WSF has the impact of “invigorating the spleen and benefiting the stomach, clearing heat and promoting diuresis”. Which is consistent with the theoretical basis of TCM for the treatment and prevention of fatty liver disease. Although WSF has demonstrated favorable efficacy in the long-term clinical practice of Prof. Kungen Wang, and our previous studies have shown that WSF treatment effectively protected against lipid metabolism disorders and liver inflammation injury in HSHFD-induced NAFLD mice, and its molecular mechanism might be via suppressing the TLR4/NF-κB/COX-2 inflammatory pathway to reduce the release of inflammatory cytokines in the liver[3]. The specific actions and mechanisms of WSF in lipid metabolism disorders needs further investigation.

When individuals persistently engage in unhealthy habits such as an HSHFD, the balance of gut flora is disrupted[4, 5]. Numerous studies have indicated that gut flora dysbiosis is one of the causative factors of MAFLD[6, 7]. It has been demonstrated that the gut flora is a significant contributing factor to the development of MAFLD, irrespective of obesity status. An imbalance in the gut flora is associated with pathological states such as lipid accumulation, decreased insulin sensitivity, and inflammatory responses[8]. The gut flora is essential for producing secondary bile acids (SBAs), and its deconjugation of BAs inhibits their reabsorption from the small intestine through the apical sodium-dependent BA transporter (ASBT). The deconjugation of BAs is carried out by gut flora with bile salt hydrolase (BSH) activity. Metagenomic analyses have revealed that BSH is widely present in major human gut flora, encompassing genera such as *Lactobacillus*, *Bifidobacteria*, *Clostridia*, and *Bacteroides*[9-12]. Disturbed gut flora alters BA composition and subsequently leads to impaired metabolism through FXR-dependent pathways, including induction of de novo lipogenesis, affecting the expression of enzymes involved BA synthesis (e.g. CYP7A1, CYP27A1) and initiating inflammatory responses in the liver[13-15].

Studies have shown that the degree of progression of MAFLD is positively correlated with serum TBA levels[16, 17]. BAs are crucial signalling molecules, and the BA receptor signalling pathway is intricately linked to the regulation of glucose and lipid metabolism[18, 19]. As multifunctional signalling molecules, BAs regulate glucose, lipid, and energy homeostasis mainly through the regulation of the farnesoid X receptor (FXR). FXR is mainly expressed in the liver and enterocytes, is a BA sensor that negatively feedback regulates BA synthesis and plays an important role in lipid metabolism[20]. In the liver, the activation of FXR by BAs triggers the expression of the small heterodimer partner (SHP). This, in turn, negatively regulates the classical BA synthesis

pathway, which is primarily controlled by the enzymes CYP7A1 and CYP8B1[21]. Hepatic FXR also positively regulates bile salt export pump (BSEP) expression, attenuating liver BA accumulation[22]. In addition to its effects in the liver, FXR is activated by BAs in the ileum, which induces the expression of fibroblast growth factor 15 (FGF15; FGF19 in humans). FGF15/19 reaches the liver through the portal bloodstream and binds to fibroblast growth factor receptor 4 (FGFR4), which inhibits the expression of BA synthase enzymes[23-25].

In conclusion, disturbance of BA metabolism, induced by imbalances in the gut flora, represents a significant pathway in the onset of MAFLD. HSHFD-induced gut flora dysbiosis further contributes to the disruption of BA metabolism and triggers hepatic steatosis. Therefore, regulating gut flora and FXR-based pathways may be a novel approach to the treatment of MAFLD.

2. Materials and methods

2.1. Chemical and biological reagents

TC (230629201), TG (230809201), HDL-c (230803301), AST (230911101), ALT (230612103), glucose (GLU, 230804101), non-esterified fatty acids (NEFA, 230704102), and total bile acid (TBA, 230509102) test kits were obtained from Medicalsystem Biotechnology Co., Ltd. (Zhejiang, China). Interleukin (IL)-1β ELISA kit (MM-0047R1), IL-6 ELISA kit (MM-0190R1), and tumor necrosis factor (TNF)-α ELISA kit (MM-0180R1) were obtained from Meimian Industrial Co., Ltd. (Jiangsu, China). Insulin ELISA kit (H203-1-2) was obtained from Nanjing Jiancheng Bioengineering Institute Co., Ltd. (Jiangsu, China). PPAR-α antibody (66826-1-Ig) was obtained from Proteintech Group Inc. (Illinois, USA). Sterol regulatory element binding protein (SREBP)-1c antibody (23BP14088I14) was obtained from Boster Biological Technology Co., Ltd. (Zhejiang, China). Acetyl-CoA carboxylase (ACC) antibody (X0710P) and stearoyl-CoA desaturase (SCD)-1 antibody (W0406P) were obtained from Diag Biotechnology Co., Ltd. (Zhejiang, China). FXR antibody (bs-12867R) and SHP antibody (bs-4311R) were obtained from Bioss Biotechnology Co., Ltd. (Beijing, China). SREBP-2 antibody (12x4294) was obtained from Affinity Biosciences Co., Ltd. (Jiangsu, China). β-actin antibody (T40104S) was obtained from Abmart Shanghai Co. Ltd. (Shanghai, China). RNA extraction (G3013), Water Nuclease-Free (G4700), RNA Storage Solution (G3029), One-Step gDNA Remover (G3337), and 2×Universal Blue SYBR Green qPCR Master Mix (G3326) were obtained from Wuhan Servicebio Technology Co., Ltd. (Wuhan, China). BAs standards were listed in **Supplementary Table 1**.

2.2. Animals

48 SD rats (SPF, male, 6 weeks old, 180 ± 20 g) were purchased from Shanghai SLAC Laboratory Animal Co. Ltd. (Shanghai, China; SCXK (Hu) 2022-0004). This study and all animal experimental procedures were approved by the Animal Center of ZJUT (approval number: MGS20231017141). All animal housing and experiments were conducted in strict accordance with

the Guide for the Care and Use of Laboratory Animals (revised in 2011).

2.3. Preparation of drugs and quality control

Metformin Hydrochloride Tablets (MET; ACL5650; 500mg/tablet) were obtained from Merck Pharmaceutical Manufacturing Co., Ltd. (Jiangsu, China) and diluted to a concentration of 10.42 mg/mL.

The herbs in the WSF were all obtained from Zhejiang Inte Pharmaceutical Co., Ltd. WSF was prepared by the Institute of TCM and Health Products of ZJUT. The herbs in the WSF are listed in **Supplementary Table 2**. The detailed procedure is as follows: proportionally weigh the herbs and add 10 times (v/m) pure water. Soak the mixture for 1 hour, followed by heating to reflux for 1 hour. Centrifuge the solution at 3000 rpm for 5 minutes, and then collect the supernatant. Add 10 times pure water again for a second extraction. Combine the extracts and concentrate to a final concentration of 1.98 g/mL and refrigerated at -20 ℃.

The quality control of WSF can be found in our earlier research[3]. HPLC-Q-TOF/MS analysis of WSF are showed in **Supplementary Figure 1**, and the information of components identified tentatively in WSF was listed in **Supplementary Table 3**.

2.4. Animal modeling of MAFLD and intervention strategies

After one week of adaptive feeding, 48 SD rats were randomly divided into six groups based on their body weight and blood lipid levels (N = 8): a normal control group (NC), a MAFLD model control group (MC), a MET group (MET, 104.2 mg/kg, i.g., qd.), and three WSF groups (W-L, 4.9 g/kg; W-M, 9.9 g/kg; W-H, 19.8 g/kg; i.g., qd.). The NC group was fed a chow diet (P1300F, 3.6 kcal/g, calorie ratio: 21.73% protein, 11.40% fat, 66.87% carbohydrates; Shanghai SLAC Laboratory Animal Co. Ltd., Shanghai, China). All other groups were fed an HSHFD (TP0860, 4.2 kcal/g, 15% fat, 15% fructose, 0.2% cholesterol added, calorie ratio: 37% fat, 14% sugar; Trophic Animal Feed High-Tech Co., Ltd., Jiangsu, China).

Dosing started 10 weeks after modeling; the NC group and MC group were given pure water, and other groups were given corresponding drugs (10 mL/kg) for 8 weeks.

2.5. Biochemical assays

The animals were fasted overnight every 4 weeks, and blood samples were collected from the ophthalmic venous plexus. The blood was centrifuged at 3000 rpm for 10 min twice to collect serum. 100 mg liver tissue was immersed in 0 ℃ ethanol and subsequently homogenized to create a 10% (w/v) homogenate. The homogenate was then subjected to centrifugation at 3000 rpm for two rounds of 10 minutes each to obtain the supernatant.

Serum ALT, AST, TC, TG, HDL-c, NEFA, TBA, and liver TC, TG, NEFA were detected with corresponding kits by Hitachi 7020 Automatic Biochemical Analyzer (Hitachi, Shanghai, China). LDL-c levels were calculated: LDL-c = TC — HDL-c — TG ÷ 2.2[26].

2.6. Oral glucose tolerance test (OGTT)

After treatment for 8 weeks, rats were fasted overnight and given 20% glucose solution (i.g., 2.0 g/kg). Blood was collected from the tail at 0 min, 30 min, 60 min, and 120 min, respectively. The blood glucose levels were measured using a Roche blood glucose meter (ACCU-CHEK Guide) and recorded as G_0-G_{120}, respectively. Area under the curve (AUC) = $(G_0 + 2G_{30} + 3G_{60} + 2G_{120}) \div 2 \times 0.5$ h.

2.7. ELISA analysis

After treatment for 8 weeks, 80 mg liver tissue was processed into a 10% (w/v) homogenate using PBS (0 ℃, pH 7.4, 0.01 M). This homogenate was subjected to centrifugation at 12,000 rpm for two consecutive intervals of 5 minutes each. Serum was collected following centrifugation of blood samples obtained from the ophthalmic venous plexus at 3000 rpm for two 10-minute rounds. ELISA kits were used to determine the levels of liver IL-1β, IL-6, TNF-α, and serum fasting insulin (FINS), according to the manufacturer's instructions.

2.8. Histopathological examination

Histopathological assessments, including H&E, Masson's trichrome, Oil Red O, and periodic acid-Schiff (PAS) staining, were conducted as previously described in our earlier studies[27, 28]. The perinephric adipose (PA), epididymal adipose (EA), and liver tissues were preserved in 10% neutral-buffered formalin, followed by dehydration using a Sakura Tissue-Tek VIP 5Jr (Sakura Finetek Japan Kabushiki Kaisha, Japan). The dehydrated tissues were then embedded in paraffin with a Meiko EC360 embedding system (Meiko, China) and cut into 4 μm sections using a Leica RM2245 microtome (Leica, Japan). These sections were subsequently subjected to staining with H&E, Masson's trichrome, and PAS.

Liver tissue sections, cut to a thickness of 8 μm using cryosectioning, were stained with Oil Red O and counterstained with hematoxylin. Following sealing and drying, the histopathological alterations in these sections were captured using a BX43 microscope (Olympus, Japan).

2.9. BAs targeted metabolomics

2.9.1 Fecal excretion of BAs in 24 h

The rats were housed in metabolic cages for a 24-hour period, during which feces were collected and weighed. The collected feces were thoroughly homogenized by adding pre-cooled saline at a ratio of 30 times (V/M). This mixture was then centrifuged at 5000 rpm, and the supernatant was separated. TBA levels in the supernatant were quantified using a Hitachi 7020 Automatic Biochemical Analyzer (Hitachi, Shanghai, China).

2.9.2 Preparation of bile acid standards

The 47 bile acid standards were accurately weighed, and the single standard mother solutions were prepared in methanol. Measure each mother liquor to formulate a mixed standard and dilute

with 50% acetonitrile to prepare a working standard solution. Prepare single-standard mother solutions of isotope standards (CDCA-D4, CA-D4) in methanol. Mixed isotope standards were prepared and diluted in methanol to 2000 ng/mL (labeled as internal standard working solution 1) and 200 ng/mL (labeled as internal standard working solution 2). Take the above working standard solution, add the internal standard working solution in a volume ratio of 1:1, and mix well to obtain the linear solutions L_1-L_{12} with concentrations of 0.2, 0.5, 1, 2, 5, 10, 20, 50, 100, 200, 500, and 1000 ng/ml, respectively.

2.9.3 Extraction of liver BAs

25 mg Liver, add 50 μL internal standard working solution 2 (200 ng/mL), add 350 μL extraction solution (water:methanol = 1:4), grind 6 min (-10 ℃, 50 Hz), sonicate 30 min (5 ℃, 40 KHz), leave at -20 ℃ for 30 min, centrifuge at 4 ℃ and 13,000g for 15 min and collect the supernatant. Blow dry under nitrogen, add 100 μL 50% acetonitrile/water to redissolve, vortex mix for 30 s, low-temperature sonication for 10 min (5 ℃, 40 KHz), centrifuge at 13000g for 15 min at 4 ℃, and collect the supernatant.

2.9.4 Detection and analysis

The analysis for both qualitative and quantitative assessment of 47 BAs was conducted using a UPLC-Qtrap 6500 system (AB SCIEX, USA), equipped with a Waters BEH C18 column (150× 2.1 mm, 1.7 μm). The column temperature was maintained at 50 ℃. The injection volume was set at 5 μL, and the flow rate was adjusted to 0.4 mL/min. Mobile phase A consisted of an aqueous solution containing 0.1% formic acid (v/v), while mobile phase B was formulated as an acetonitrile solution containing 0.1% formic acid (v/v). The gradient elution procedure was as follows: 0-0.5 min, 95-90% A; 0.5-1 min, 90-80% A; 1-2 min, 80-72% A; 2-8 min, 72% A; 8-11 min, 72-67% A; 11-20 min, 67-55% A; 20-23%, 55-50% A; 23-29 min, 50-20% A; 29-29.01 min, 20-0% A; 29.01-31 min, 0% A; 31-31.01 min, 0-95% A; 31.01-33 min, 95% A. The mass spectra were detected in negative ion mode: the spray voltage is -4.5 kV, the spray gas is 50 psi, the auxiliary heating gas is 50 psi, the air curtain gas is 35 psi, the collision gas is Medium, and the ion source temperature is 550 °C.

Default parameters were used in the SCIEX OS to identify and integrate individual ion fragments with manual inspection automatically. A linear regression standard curve was plotted using the ratio of the analyte's peak area to the internal standard's peak area as the vertical coordinate and the analyte concentration as the horizontal coordinate. BA content (ng/mg)=(C×V×DF)÷W (C: measured concentration (ng/mL); V: metered volume (mL); W: sample weight (mg); DF: dilution factor).

2.10. 16S rRNA sequencing

The method of gut flora analysis is consistent with our previous study[29]. In summary, the

V3-V4 hypervariable regions of the bacterial 16S rRNA gene were amplified using the primers 338F (5'-ACTCCTACGGGAGGCAGCAG-3') and 806R (5'-GGACTACHVG GGTWTCTAAT-3'), with the amplification conducted on a GeneAmp 9700 PCR system (ABI, USA). The amplified PCR products were then extracted from a 2% agarose gel and purified using the AxyPrep DNA Gel Extraction Kit (Axygen Biosciences, USA), with their concentrations determined using QuantiFluor™-ST (Promega, USA). The purified DNA samples were sequenced on the Illumina MiSeq platform (Illumina, USA) following standard protocols by Majorbio Bio-Pharm Technology Co. Ltd. (Shanghai, China). Operational taxonomic units (OTUs) were identified by clustering sequences with a 97% similarity threshold using UPARSE (version 7.0.1090, available at http://drive5.com/uparse/). Taxonomic assignments were carried out using the RDP Classifier algorithm (http://rdp.cme.msu.edu/) against the Silva 16S rRNA database (Release 138, http://www.arb-silva.de), with a confidence threshold set at 70%. Data analysis was performed on the Major Cloud platform (http://cloud.majorbio.com), including analysis of the community structure at the generic level, calculation of alpha diversity, and assessment of beta diversity at the generic level.

2.11. Western Blot

The expression of FXR, SHP, PPAR-α, SCD-1, and SREBP-1 in the liver was determined by WB as described previously[27]. Briefly, the extracted proteins were separated by SDS-PAGE and transferred to a PVDF membrane. The membrane was then blocked with 5% BSA for 2 hours at room tempreture and incubated with primary antibodies for 12 hours at 4 °C. Following incubation with HRP-conjugated secondary antibodies for 2 hours at room tempreture, the protein bands were visualized using enhanced chemiluminescence (ECL) reagent.

2.12. RT-qPCR

The expression of ileum FXR, FGF15, ASBT, liver FGFR4, BSEP, sodium taurocholate cotransporting polypeptide (NTCP), CYP7A1, CYP8B1, CYP27A1 and the reference gene GAPDH were analyzed by RT-qPCR as described previously[30]. Total RNA was isolated from ileum and liver tissues using RNA extraction (G3013, Servicebio Technology Co., Ltd., Wuhan, China). RT-qPCR analysis was conducted on the samples utilizing a CFX Connect Real-Time PCR Detection System (BIO-RAD, USA), with SYBR green master (G3326, Servicebio Technology Co., Ltd., Wuhan, China). Rat-specific primers were designed by Servicebio Technology Co., Ltd. (Wuhan, China). The PCR conditions were set as follows: pre-denaturation at 95 ℃ for 30 seconds; denaturation at 95 ℃ for 15 seconds, annealing/extension at 60 ℃ for 30 seconds for 40 cycles; 65 ℃ to 95 ℃ melting curve detection, and fluorescence signals were collected once for each 0.5 ℃ temperature increase. The primer information is given in **Table 1**.

Table 1 Primer series of targer mRNA in rat

Genes	Sequences (5'-3')	Tissues	Primer length (bp)
CYP7A1	Forward: ATTTGGGGAATTGCCGTGTTG Reverse: CACAGCCCAGGTACGGAATC	Liver	115
CYP8B1	Forward: GAAGTTCCGCAGATTTGACCTA Reverse: CCCAACCAGTTACTTATGCCG	Liver	156
CYP27A1	Forward: GAGACTGTCGGCACCTTTCCT Reverse: ATGTGGGCAAAGTCCTTGTTCT	Liver	179
FGFR4	Forward: GTCTACCCACAGCAAGCACC Reverse: ATCACCAGGCTCCAGTGTTG	Liver	212
BSEP	Forward: TGACACTACCTGAAAGGGTTGTT Reverse: GCGCACACACTTCCCATAAA	Liver	237
NTCP	Forward: CCTACGTCCTCAAGGCAGG Reverse: GTTTCCATGCTGATGGTGCG	Liver	220
FXR	Forward: TGAGGGCTGCAAAGGTTTCT Reverse: TCGCTGTCGTCCTCATTAGC	Ileum	258
FGF15	Forward: GCTCAGCAATCCCAGTCTGT Reverse: CCTCCGAGTAGCGAATCAGC	Ileum	289
ASBT	Forward: ACAAATGGCCACAAAAAGCGA Reverse: ACTGTTCGGCACCTGTACCA	Ileum	223
GAPDH	Forward: CTGGAGAAACCTGCCAAGTATG Reverse: GGTGGAAGAATGGGAGTTGCT	Liver/Ileum	138

2.13. Immunofluorescence observation

The expression of liver ACC, SCD-1, SREBP-1c, and SREBP-2 was determined by IF, according to our previous study[31]. Tissue sections were deparaffinized, antigen retrieval and blocking were performed, followed by incubation with the appropriate primary antibodies at 4 °C overnight. FITC-conjugated secondary antibody was then added and sections were incubated in the absence of light. Nuclei were stained with DAPI for 5 minutes at room temperature in the absence of light. The sections were imaged using a BX43 microscope (Olympus, Japan) at a magnification of 400×.

2.14. Statistical analysis

All data were presented as mean ± standard deviation (SD). Statistical analysis and data visualization were conducted using SPSS 27.0 and GraphPad Prism 9.5.0, respectively. One-way analysis of variance (ANOVA) was employed to determine significant differences among the measured traits. When the hypothesis of homogeneity of variance was satisfied, the LSD *t*-test was applied; otherwise, the Tamhane'T2 *t*-test was applied. A value of $P < 0.05$ was considered statistically significant.

3. Results

3.1. WSF alleviated the pathological manifestations of MAFLD model rats

Ten weeks after modeling, the body weight of rats in the MC group exhibited a significant

rise of 37.0% relative to the NC group ($P < 0.01$). After two weeks of treatment, the W-H group had a notable 7.8% decrease in body weight relative to the MC group. ($P < 0.05$).

Following eight weeks of treatment, the W-H group exhibited markedly reduced body weight, body weight gain rate, and Lee's index in comparison to the MC group ($P < 0.05$), with respective changes of 8.9%, 15.0%, and 2.5%. Despite a declining tendency in body weight among the rats in the W-L and W-M groups, the differences were not statistically significant when compared to the MC group. The body weight gain rate in the W-H group was lower than that in the W-L and MET groups ($P < 0.05$), while it did not significantly differ from that of the W-M group (**Figure 2**). It was suggested that WSF could improve signs of obesity in MAFLD model rats, and the best effect was seen at a dose of 19.8 g/kg.

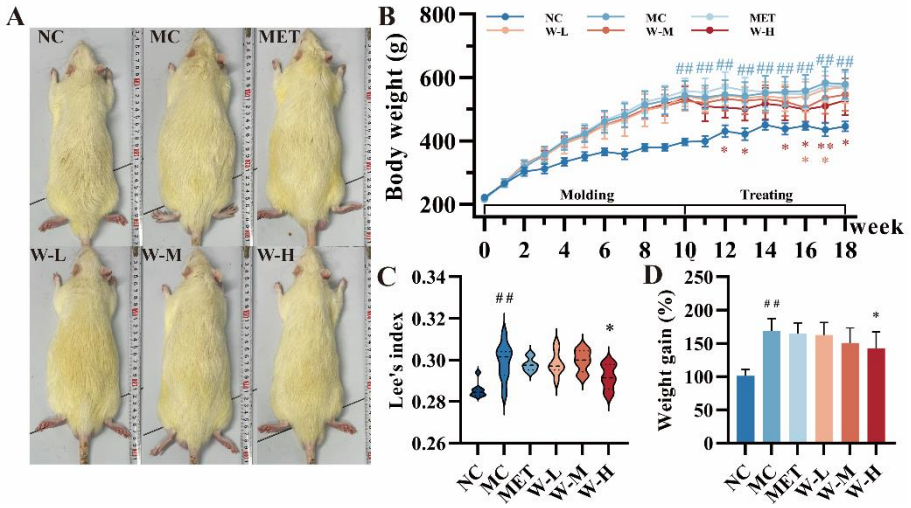

Figure 2 Effects of WSF on the general physical signs of model rats. (A) Appearances of rats. (B) Body weight. (C) Lee's index. (D)Weight gain in 18 weeks. # ($P < 0.05$), ## ($P < 0.01$) vs. NC; * ($P < 0.05$), ** ($P < 0.01$) vs. MC.

3.2. WSF improved serum transaminases in MAFLD model rats

In comparison to the NC group, serum AST and ALT levels significantly elevated ($P < 0.05$) in the MC group after ten weeks of modeling, with increases of 29.6% and 32.4%, respectively. Following 18 weeks of modelling, blood AST and ALT levels in the MC group of rats increased by 53.1% and 76.5%, respectively ($P < 0.05$, 0.01). It was suggested that the liver dysfunction of the model rats worsened with the prolongation of the modeling time.

In comparison to the MC group, following four weeks of treatment, serum AST levels exhibited a downward trend ($P = 0.080$), and serum ALT was significantly reduced ($P < 0.01$) in the W-M group of rats, with changes of 17.1% and 37.5%, respectively; while W-H significantly reduced serum AST and ALT in the MAFLD rats ($P < 0.05$, 0.01), with changes of 23.5% and 40.7%, respectively. After eight weeks of medication, blood ALT and AST levels were considerably decreased in all WSF groups compared to the MC group ($P < 0.01$). There was no

substantial difference among the three dosage groups (**Figure 3**). The results suggest that WSF can significantly reduce liver injury in MAFLD model rats and that the 19.8 g/kg dose has an earlier onset of action.

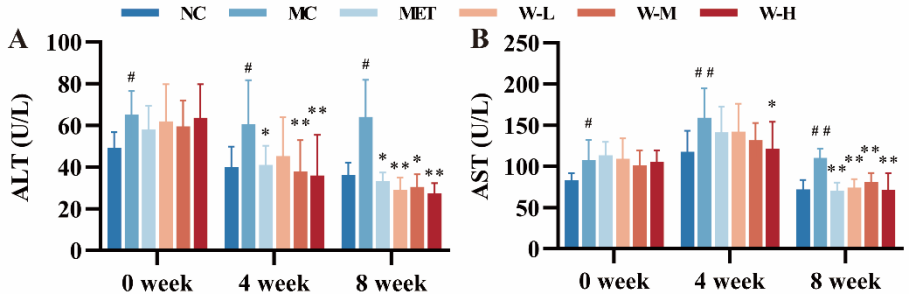

Figure 3 Effects of WSF on the liver function in model rats. (A) Serum ALT. (B) Serum AST. # ($P < 0.05$), ## ($P < 0.01$) vs. NC; * ($P < 0.05$), ** ($P < 0.01$) vs. MC.

3.3. WSF improved lipid metabolism in MAFLD model rats

Compared with the NC group, after ten weeks of modeling, serum TC, TG, and LDL-c increased by 44.6%, 96.0%, and 63.0%, respectively ($P < 0.05$, 0.01), and serum HDL-c decreased by 46.7% ($P < 0.01$) in the MC group. After eighteen weeks of modeling, in addition to the abnormalities of serum TC, TG, HDL-c, and LDL-c, serum NEFA also increased significantly by 71.0% in the MC group ($P < 0.01$). Hepatic TC, TG, and NEFA increased by 1.33-fold, 1.42-fold, and 2.86-fold in the MC group ($P < 0.01$), respectively.

Following eight weeks of treatment, sreum TC, TG, LDL-c, and NEFA were significantly reduced in all WSF groups relative to the MC group ($P < 0.01$); additionally, serum HDL-c in the W-H group exhibited a significant increase of 27.4% ($P < 0.05$). Furthermore, both the W-M and W-H groups demonstrated significant reductions in hepatic TG and NEFA levels ($P < 0.05$, 0.01), and W-H also decreased hepatic TC levels in the model rats ($P < 0.05$; **Figure 4**).

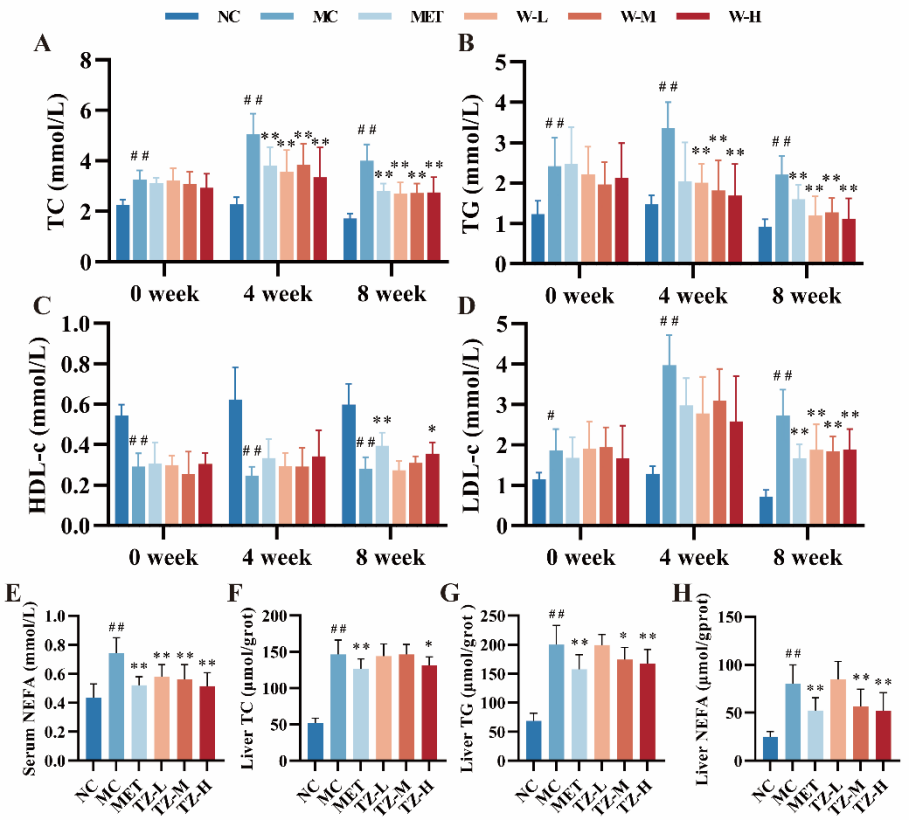

Figure 4 Effects of WSF on the lipid metabolism in model rats. (A) Serum TC. (B) Serum TG. (C)Serum HDL-c. (D) Serum LDL-c. (E) Serum NEFA. (F) Liver TC. (G) Liver TG. (H) Liver NEFA. # ($P < 0.05$), ## ($P < 0.01$) vs. NC; * ($P < 0.05$), ** ($P < 0.01$) vs. MC.

3.4. WSF attenuated insulin resistance in MAFLD model rats

After eighteen weeks of modeling, the MC group rats exhibited significantly elevated fasting blood glucose, fasting insulin, and insulin resistance index compared to the NC group ($P < 0.01$); the OGTT indicated impaired glucose tolerance and a considerably higher AUC in the MC group ($P < 0.01$). In comparison to the MC group, the fasting blood glucose levels of rats in the W-M and W-H groups were considerably diminished after eight weeks of treatment ($P < 0.05$, 0.01), with a more pronounced drop observed in the W-H group. WSF reduced the AUC across all treated groups ($P < 0.05$, 0.01). Furthermore, the serum FINS levels in the W-M and W-H groups exhibited a decline of 5.1% and 8.2%, respectively. The insulin resistance index of W-H rats was markedly diminished ($P < 0.01$; **Figure 5**).

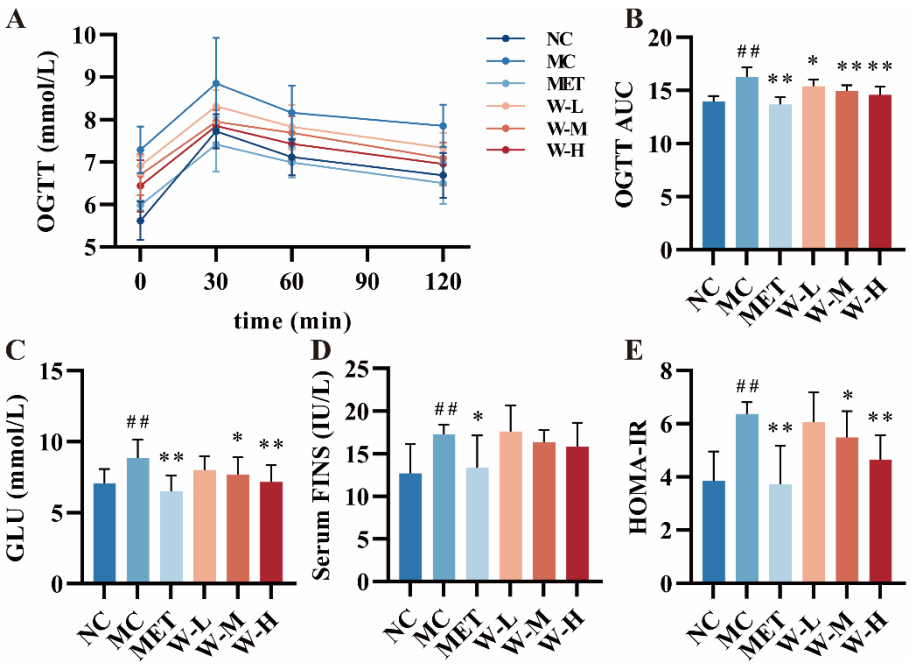

Figure 5 Effects of WSF on the glucose metabolism in model rats. (A) OGTT. (B) OGTT AUC. (C) FBG. (D) FINS. (E) HOMA-IR. # ($P < 0.05$), ## ($P < 0.01$) vs. NC; * ($P < 0.05$), ** ($P < 0.01$) vs. MC.

3.5. WSF reduced visceral adipose accumulation in MAFLD model rats

Following eighteen weeks of modeling, the volumes of EA and PA in the MC group were significantly greater than those in the NC group; the weights of EA and PA increased by 108.2% and 265.8%, respectively ($P < 0.01$), and the lipid/brain ratios of EA and PA were significantly elevated ($P < 0.05$, 0.01). The results of H&E staining showed that the adipocytes in the NC group were uniformly distributed in a honeycomb shape with small cell diameters; the area of adipocytes in the MC group was significantly increased, and the diameter of EA cells and PA cells were increased by 39.5% and 52.5%, respectively ($P < 0.01$).

Following eight weeks of administration, the volumes of EA and PA in the W-H group were reduced compared to the MC group. The weights of EA and PA were reduced by 22.4% and 27.8%, respectively ($P = 0.064$, 0.055), corresponding to the trend of lowering the lipid/brain ratio ($P = 0.087$, 0.066). The diameters of EA and PA cells in the W-H group were shortened by 26.0% and 16.7%, respectively ($P < 0.01$; **Figure 6**). It was suggested that WSF could reduce visceral fat accumulation and ameliorate abdominal obesity in MAFLD model rats.

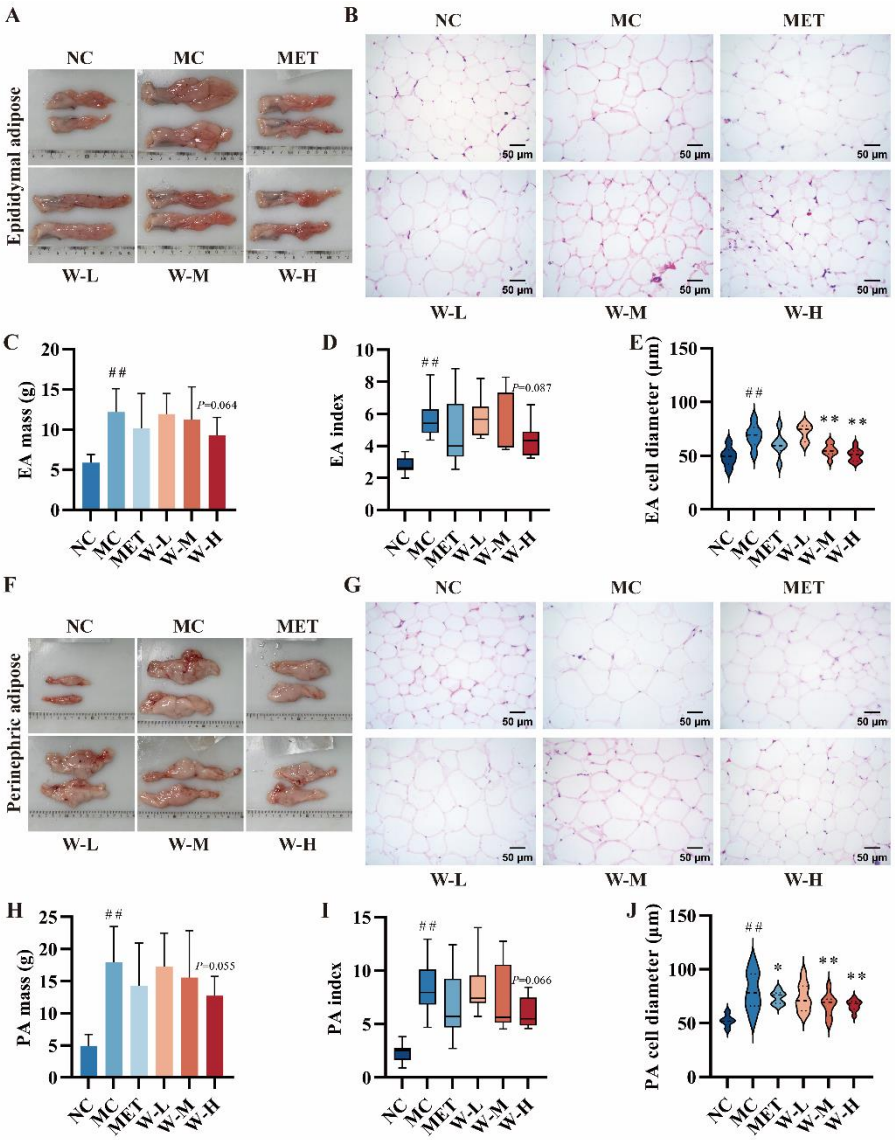

Figure 6 Effects of WSF on the adipose tissue in model rats. (A) Appearances of EA. (B) H&E staining of EA (400×). (C) EA mass. (D) EA-brain ratio. (E) EA cell diameter. (F) Appearances of PA. (G) H&E staining of PA (400×). (H) PA mass. (I) PA-brain ratio. (J) PA cell diameter. # ($P < 0.05$), ## ($P < 0.01$) vs. NC; * ($P < 0.05$), ** ($P < 0.01$) vs. MC.

3.6. WSF attenuated liver lesions in MAFLD model rats

Following eighteen weeks of modeling, the liver volume of rats in the MC group was markedly greater than that of the NC group. The liver weight and liver/brain ratio were increased by 83.6% and 80.1%, respectively ($P < 0.01$; **Figure 7 A, F-G**). Intracellular lipid droplets in hepatocytes showed diffuse and granular accumulation. The area stained with Oil Red O in the liver significantly increased ($P < 0.01$). However, there was no abnormal increase in collagen deposition within the liver (**Figure 7 B-D, H**). In the MC group, most hepatocytes showed faint glycogen staining with significant glycogen depletion, and the density of hepatic glycogen was significantly reduced ($P < 0.01$; **Figure 7 E, I**). The levels of liver inflammatory factors IL-1β, IL-6, and TNF-α in the MC

group increased by 40.4%, 70.3%, and 79.2%, respectively($P < 0.01$; **Figure 7 J-L**). These results indicated that the livers of MAFLD model rats exhibited severe steatosis and inflammatory response but did not progress to fibrosis.

After eight weeks of administration, the liver weight and the liver/brain ratio of W-H rats were significantly reduced compared to the MC group, with changes of 16.5% and 15.3%, respectively ($P < 0.05$; **Figure 7 F-G**). In W-H rats, lipid droplets in hepatocytes were sparsely distributed, and the area stained with Oil Red O in the liver was significantly reduced ($P < 0.05$; **Figure 7 D, H**). In the WSF treatment groups, the glycogen staining in hepatocytes was darker, indicating a significant improvement in glycogen depletion ($P < 0.01$; **Figure 7 E, I**). The levels of IL-1β, IL-6, and TNF-α in the livers of W-M and W-H rats were significantly reduced ($P < 0.05, 0.01$); the W-L dose only reduced the level of TNF-α in the model rats by 16.6% ($P < 0.05$; **Figure 7 J-L**). In conclusion, WSF can improve hepatic glucose and lipid metabolism and alleviate liver inflammation in MAFLD model rats. Further investigation of its mechanism of action is warranted.

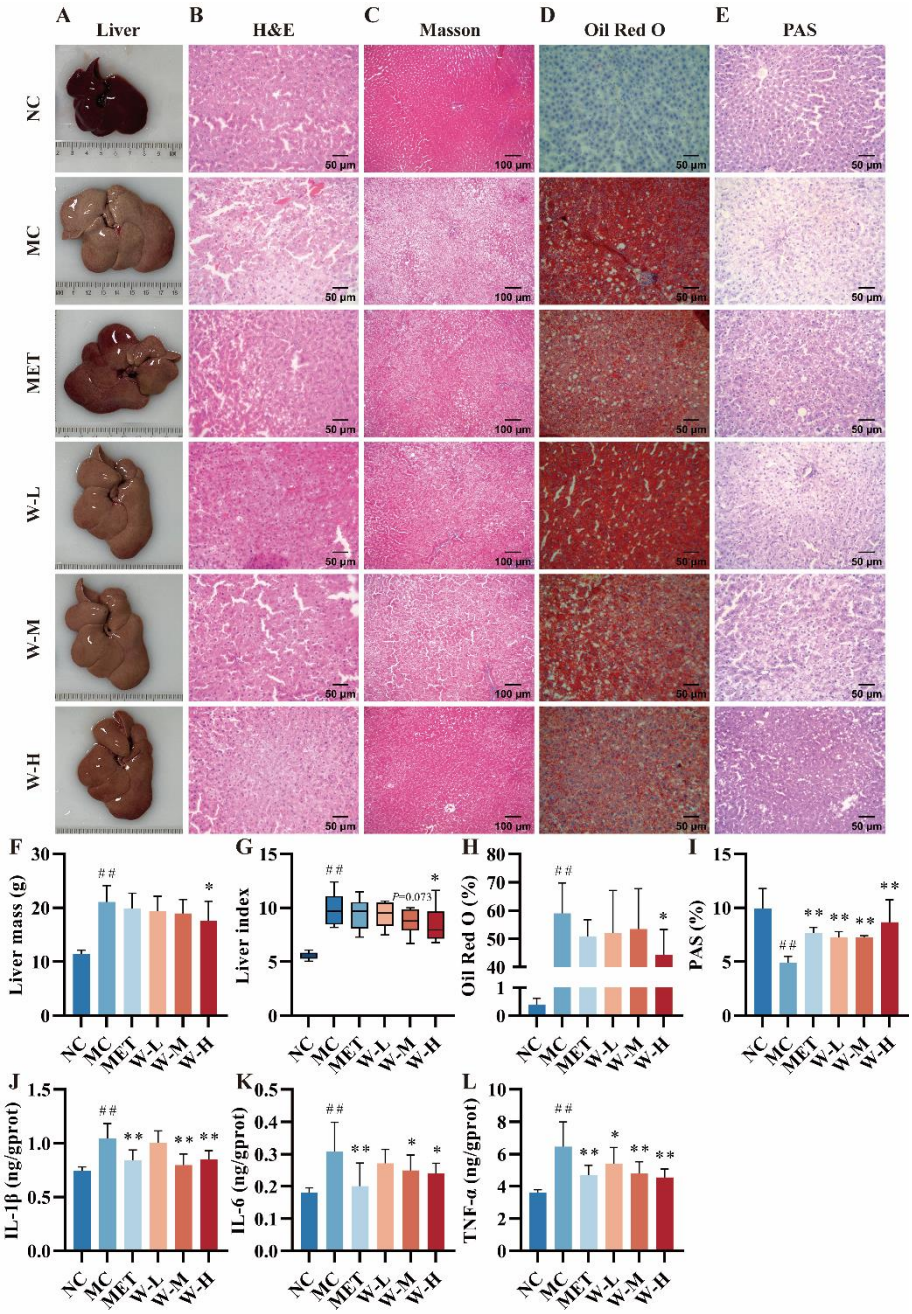

Figure 7 Effects of WSF on histopathology of the liver in model rats. (A) Appearances of liver. (B) H&E (400×). (C) Masson (200×). (D) Oil Red O (400×). (E) PAS (400×). (F) Liver mass. (G) Liver-brain ratio. (H) Percentage of Oil Red O staining area. (I) Percentage of PAS staining area. (J) Hepatic IL-1β. (K) Hepatic IL-6. (L) Hepatic TNF-α. # ($P < 0.05$), ## ($P < 0.01$) vs. NC; * ($P < 0.05$), ** ($P < 0.01$) vs. MC.

3.7. WSF modulated hepatic bile acid profile in MAFLD model rats

This experiment conducted the detection and analysis of 47 BAs. The total ion chromatogram (TIC) plot showed high separation and well-defined peak shapes for each analyte. The results are presented in the **Supplementary Figure 2**. Linear regression standard curves were constructed with the chromatographic peak area of the standard solution represented on the y-axis and the concentration on the x-axis. The linear R^2 values for all analytes were greater than 0.99, indicating

good linearity (**Supplementary Table 4**). In this experiment, a mixed standard solution was used as the quality control sample, with one quality control sample being analyzed for every 6-12 samples run. The results showed that all BAs' relative standard deviation (RSD) was less than 15% (**Supplementary Table 5**).

3.7.1. Effect of WSF on overall BAs levels

In comparison to the NC group, the serum and liver TBA levels in the MC group exhibited increases of 57.3% and 49.4%, respectively ($P < 0.01$). The daily fecal BA excretion in the MC group also increased ($P = 0.120$). Following eight weeks of treatment, blood TBA and liver TBA levels in the W-H group diminished by 57.5% and 30.0%, respectively, in comparison to the MC group ($P < 0.05$, 0.01), accompanied by a 64.6% augmentation in daily fecal BA excretion ($P < 0.01$; **Figure 8 A-C**). The findings suggested that WSF may exert a beneficial effect on MAFLD by reducing the BA pool and increasing the excretion of BA in MAFLD model rats.

The MC group had a notable increase in PBA and SBA levels in the liver, rising by 46.9% and 67.6%, respectively ($P < 0.01$). The concentration of conjugated BA also showed a notable rise of 51.3% ($P < 0.01$), with a specific increase of 65.0% in taurine-conjugated BA ($P < 0.05$). Additionally, in the MC group, the levels of CA group and DCA group in the liver increased by 119.8% and 81.8%, respectively ($P < 0.01$). Conversely, the levels of the CDCA group and UDCA group decreased by 34.2% and 54.7%, respectively ($P < 0.05$).

Liver PBAs and SBAs levels in MAFLD model rats were reduced by 26.3% and 53.1%, respectively, after WSF intervention compared with the MC group ($P < 0.05$, 0.01; **Figure 8 D-E**). WSF significantly reduced the levels of conjugated BAs in the liver of MAFLD model rats ($P < 0.01$), with a notable decrease of 40.4% in taurine-conjugated BAs ($P < 0.05$; **Figure 8 F-I**). Additionally, the levels of CA group and DCA group in the liver of MAFLD model rats decreased by 49.9% and 40.3%, respectively ($P < 0.05$, 0.01), while the levels of CDCA group and UDCA group increased by 53.8% and 171.4%, respectively ($P < 0.05$; **Figure 8 J**). These findings suggested that WSF may ameliorate MAFLD by alleviating liver bile stasis and regulating the liver BAs profile.

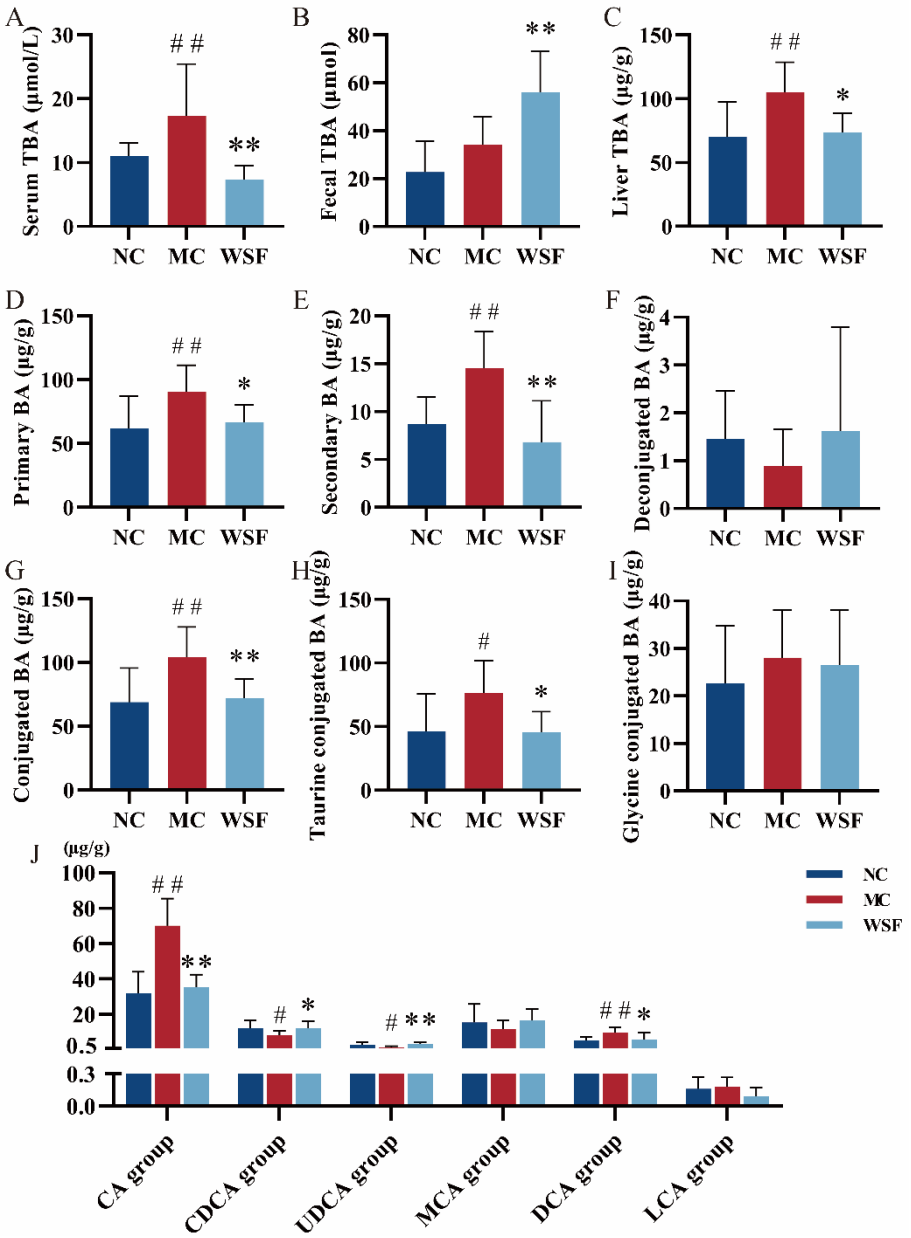

Figure 8 Effect of WSF on metabolism of hepatic BAs of model rats. (A) Serum TBA. (B) 24 h fecal TBA. (C) Liver TBA. (D) Primary BA. (E) Secondary BA. (F) Deconjugated BA. (G) Conjugated BA. (H) Taurine conjugated BA. (I) Glycine conjugated BA. (J) Major BA (CA group: CA, TCA, GCA; CDCA group: CDCA, TCDCA, GCDCA; UDCA group: UDCA, TUDCA, GUDCA; MCA group: α-MCA, β-MCA, T-α-MCA, T-β-MCA; DCA group: DCA, TDCA, GDCA; LCA group: LCA, TLCA, GLCA). # ($P < 0.05$), ## ($P < 0.01$) vs. NC; * ($P < 0.05$), ** ($P < 0.01$) vs. MC.

3.7.2. Effect of WSF on liver PBA

Compared to the NC group, in the MC group, the levels of TCA and GCA in the liver increased by 172.7% and 62.4%, respectively ($P < 0.05$, 0.01). Conversely, the levels of GCDCA and GUDCA decreased by 67.8% and 74.4%, respectively ($P < 0.05$).

In comparison to the MC group, the liver TCA in rats from the WSF group exhibited a considerable reduction ($P < 0.01$), while GCA showed a tendency towards reduction ($P = 0.078$),

with alterations of 61.9% and 28.0%, respectively. The levels of CDCA, GCDCA, UDCA, and GUDCA in the liver of the WSF group significantly increased ($P < 0.05$, 0.01), with a trend towards an increase in TUDCA ($P = 0.063$), changing by 2.05-fold, 2.33-fold, 2.17-fold, 4.68-fold, and 1.07-fold, respectively. In comparison to the NC group, no significant variations were seen in the levels of different PBAs in the liver of the WSF group (**Figure 9**). These findings suggested that WSF could regulate the levels of PBA in MAFLD model rats, thereby improving their BA profile.

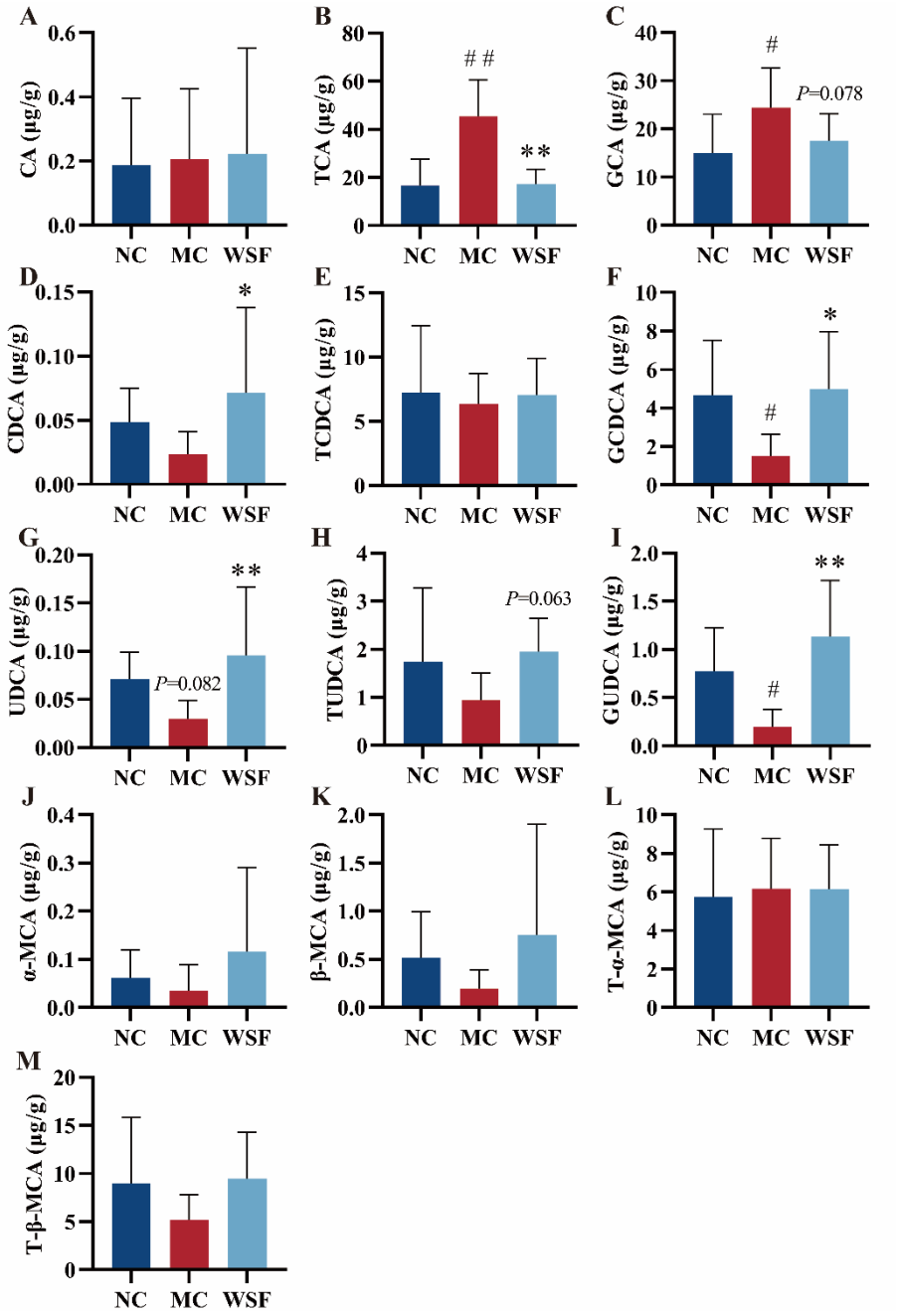

Figure 9 Effect of WSF on hepatic primary BAs of model rats. (A) CA. (B) TCA. (C) GCA. (D) CDCA. (E) TCDCA. (F) GCDCA. (G) UDCA. (H) TUDCA. (I) GUDCA. (J) α-MCA. (K) β-MCA. (L) T-α-MCA. (M) T-β-MCA. # ($P < 0.05$), ## ($P < 0.01$) vs. NC; * ($P < 0.05$), ** ($P < 0.01$) vs. MC.

3.7.3. Effect of WSF on liver SBA

Screening for differentially expressed SBA using the criteria of |FC| > 1, -log10(*P*) > 1. The results revealed lower levels of hepatic HCA, 3β-UDCA, and CDCA-24A-βGlu; and higher levels of NorCA, TDCA, and 7-DHCA in the MC group compared with the NC group.

Compared with the MC group, WSF up-regulated five SBA, including HCA, GHCA, and 3β-UDCA, and down-regulated five SBA, including TDCA, TLCA, and THDCA. The levels of HCA, 3β-UDCA, CDCA-24A-βGlu, and TDCA were altered towerd the normal levels by WSF (**Figure 10**), suggesting that WSF could alter the composition of hepatic SBAs in MAFLD model rats and regulate BA metabolism.

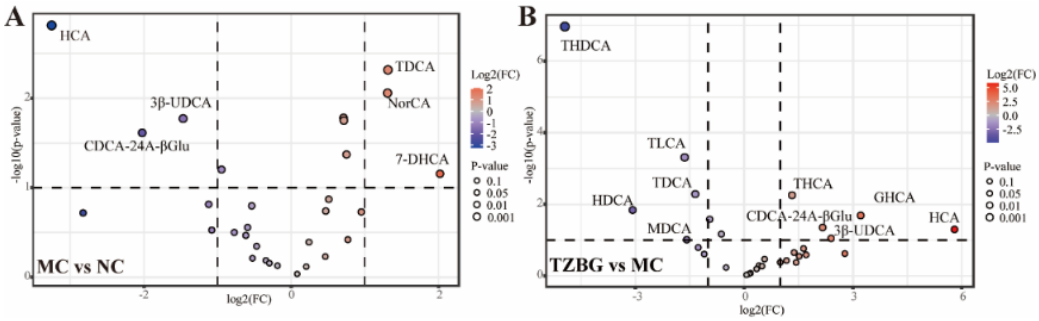

Figure 10 Effect of WSF on hepatic secondary BAs of model rats. (A) Volcano plot of SBA MC vs NC. (B) Volcano plot of SBA WSF vs MC.

3.8. WSF regulated gut flora in MAFLD model rats

3.8.1. α diversity

A total of 2,598 OTUs were analyzed. The NC group's gut flora yielded 1,845 OTUs, the MC group's gut flora yielded 1,174 OTUs, and the WSF group's gut flora yielded 1,499 OTUs (**Figure 11 A-B**). This suggested that WSF exerted a regulating influence on the gut flora abundance in MAFLD model rats.

In comparison to the NC group, the Ace, Chao, Shannon, and Sobs indices in the MC group exhibited substantial reductions ($P < 0.01$), with alterations of 45.4%, 44.4%, 14.1%, and 45.3%, respectively. Compared to the MC group, the Ace, Chao, Shannon, and Sobs indices of the gut flora in the WSF group markedly increased ($P < 0.05, 0.01$), with changes of 38.2%, 36.9%, 12.7%, and 39.8%, respectively (**Figure 11 C-F**). This indicated that WSF could enhance the diversity and evenness of gut flora in MAFLD model rats.

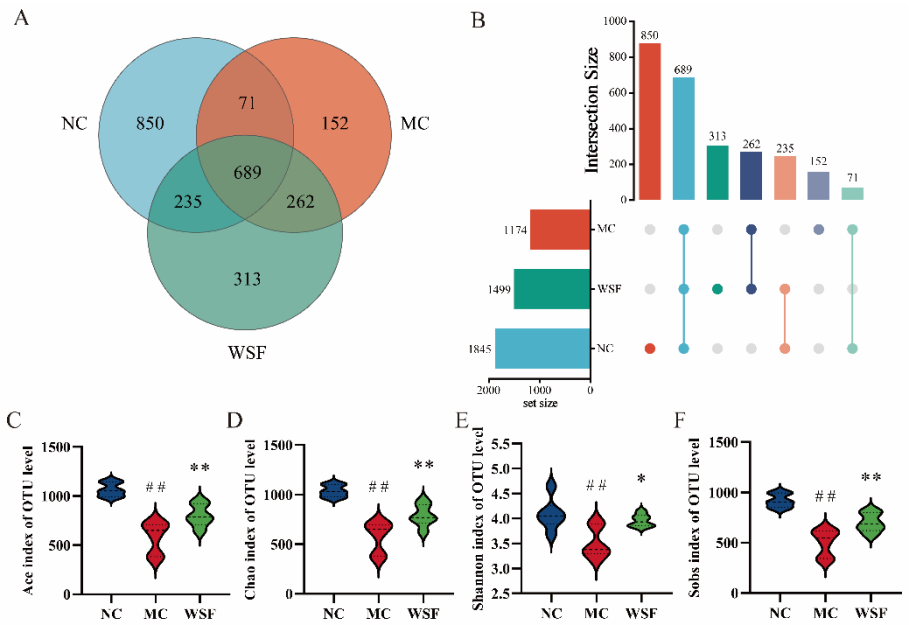

Figure 11 Effects of WSF on the α diversity of gut flora in model rats. (A) Venn. (B) Upset Venn. (C) Ace. (D) Chao. (E) Shannon. (F) Sobs. # ($P < 0.05$), ## ($P < 0.01$) vs. NC; * ($P < 0.05$), ** ($P < 0.01$) vs. MC.

3.8.2. β diversity

PCoA, NMDS, PERMANOVA, and hierarchical cluster analysis were selected to describe the β diversity of the gut flora. PCoA R = 0.7095, $P = 0.001$; NMDS stress = 0.086; PERMANOVA R^2 = 0.42473, P = 0.001; indicating that the models were reliable. Sample points were relatively clustered within groups and relatively discrete between groups, suggesting differences in species composition between groups (**Figure 12 A**). Hierarchical cluster analysis indicated a considerable separation between the NC and MC groups, implying alterations in the species composition and abundance of gut flora in MAFLD model rats. The clusters of the WSF group were distinct from those of the MC group, indicating that WSF may modulate gut flora composition in MAFLD model rats (**Figure 12 B**).

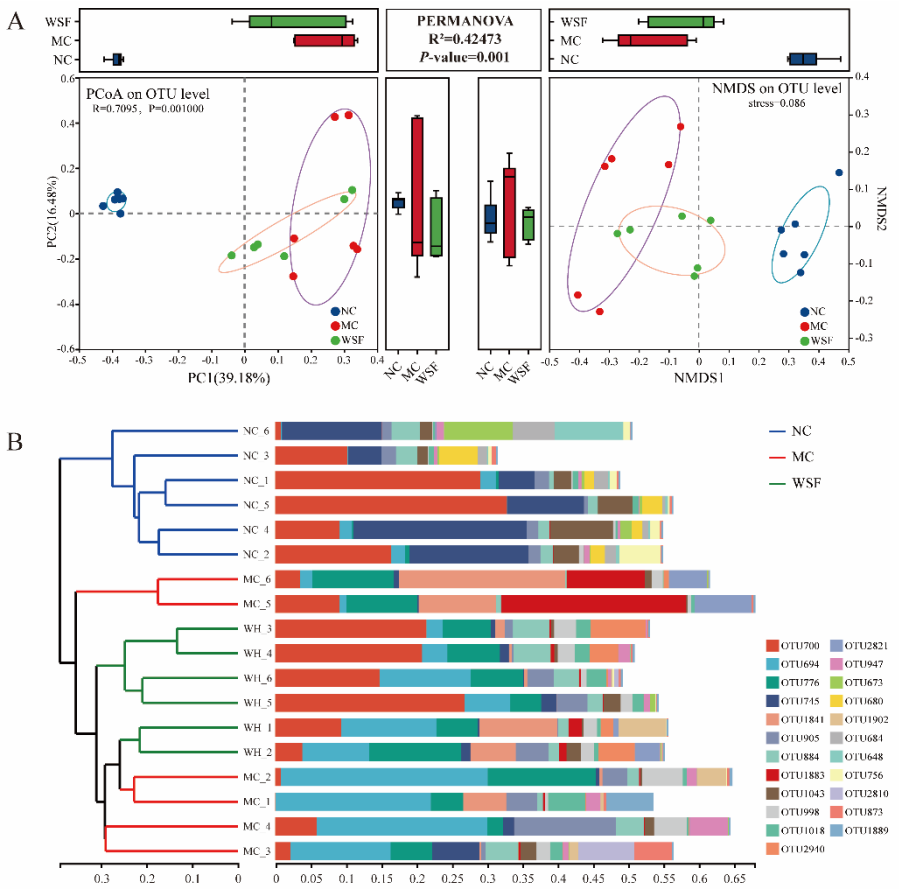

Figure 12 Effects of WSF the β diversity of gut flora in model rats. (A) PCoA, NMDS, and PERMANOVA. (B) Hierarchical cluster.

3.8.3. Differences in gut flora at the phylum level

The gut flora of the three groups was primarily composed of *Firmicutes*, *Bacteroidota*, and *Actinobacteriota* (**Figure 13 A-B**). In comparison to the NC group, the prevalence of *Bacteroidota* markedly diminished in the MC group ($P < 0.05$), although the F/B ratio and the prevalence of *Actinobacteriota* dramatically escalated ($P < 0.05$). Compared to the MC group, the abundance of *Actinobacteriota* in the W-H group dramatically dropped ($P < 0.05$), and the F/B ratio showed a downward trend, with changes of 90.1% and 28.5%, respectively (**Figure 13 C-F**).

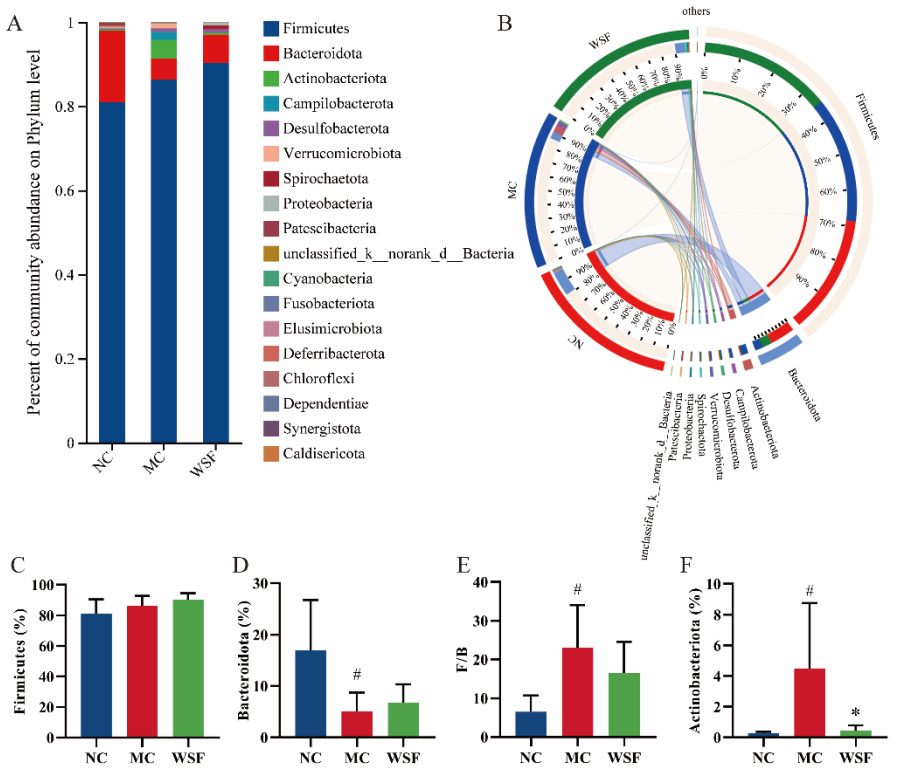

Figure 13 Effect of WSF on the phylum level of gut flora in model rats. (A) Bar plot at the phylum level. (B) Circos plot at the phylum level. (C) *Firmicutes* abundance. (D) *Bacteroidota* abundance. (E) *Firmicutes*/*Bacteroidota* ratio. (F) *Actinobacteriota* abundance. # ($P < 0.05$), ## ($P < 0.01$) vs. NC; * ($P < 0.05$), ** ($P < 0.01$) vs. MC.

3.8.4. Differences in gut flora at the genus level

To further elucidate the alterations in the gut flora of MAFLD model rats, this section presented an analysis based on genus level, examining the composition and abundance of the gut flora in the NC, MC, and WSF groups.

Compared to the NC group, the MC group demonstrated a significant increase in the relative abundances of *Blautia*, *Lachnoclostridium*, *Phascolarctobacterium*, and *UCG-008* ($P < 0.05$, 0.01, 0.001). Conversely, the relative abundances of *Lactobacillus*, norank_f__norank_o__Clostridia_UCG-014, *Ruminococcus*, and *norank_f__norank_o__RF39* in the MC group were significantly reduced ($P < 0.05$, 0.001).

Compared to the MC group, the W-H group significantly increased the relative abundances of *Lactobacillus*, *norank_f__Erysipelotrichaceae*, and *norank_f__Eubacterium_coprostanoligenes_group* at the genus level ($P < 0.05$). Conversely, the W-H group exhibited a significant reduction in the relative abundances of *Blautia*, *Akkermansia*, and *Collinsella* ($P < 0.05$, 0.01). These findings suggested that WSF could modulate the gut flora in MAFLD model rats by normalizing the relative abundances of *Lactobacillus*, *Blautia*, and *norank_f__Eubacterium_coprostanoligenes_ group* at the genus level (**Figure 14**).

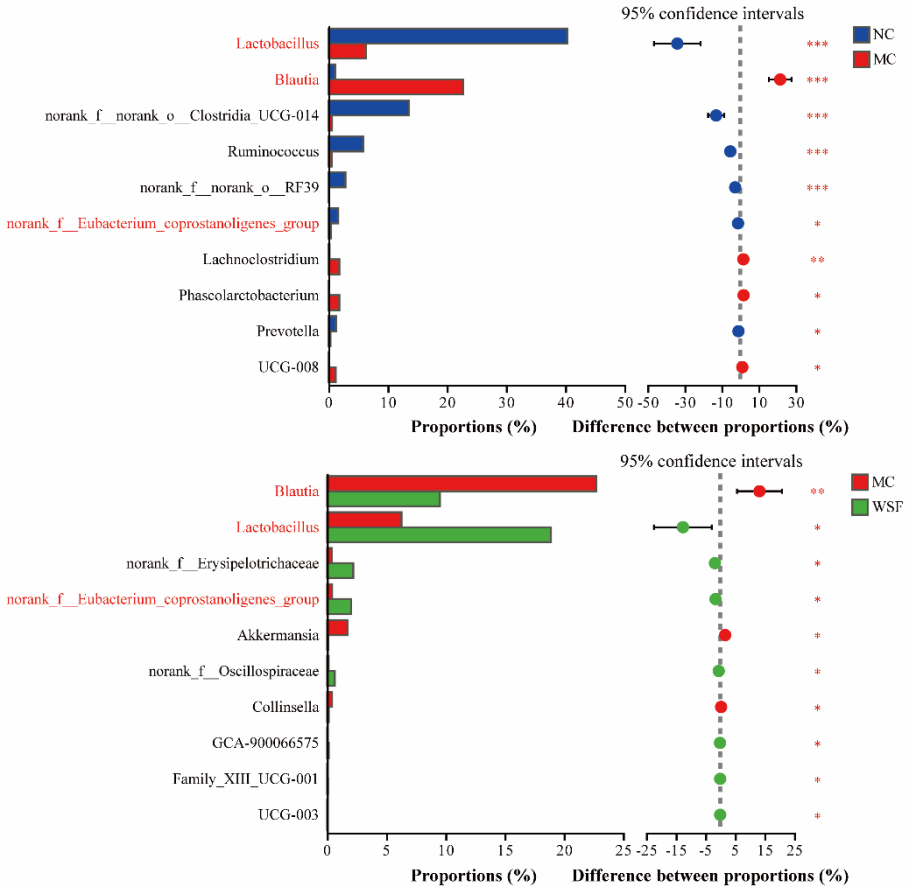

Figure 14 Effect of WSF on the species level of gut flora in model rats. (A) Differences in gut flora at the genus level NC vs MC. (B) Differences in gut flora at the genus level WSF vs MC. * ($P < 0.05$), ** ($P < 0.01$), *** ($P < 0.001$).

3.9. WSF modulated FXR pathways

Compared to the NC group, RT-qPCR results revealed a significant increase in the expression of ileal *FXR*, *FGF15* mRNA, and liver *FGFR4* mRNA in the MC group ($P < 0.01$). Furthermore, the data from WB and IF demonstrated a significant reduction in liver FXR and SHP levels in the MC group ($P < 0.01$). In contrast to the MC group, WSF rectified the changes in FXR and its associated mRNA and proteins, evidenced by a reduction in the expression of ileal *FXR*, *FGF15*, and hepatic *FGFR4* mRNA ($P < 0.05$, 0.01; **Figure 15 A-C**), alongside an elevation in the levels of liver FXR and SHP ($P < 0.05$, 0.01; **Figure 15 D-H**). The above results indicated that WSF could inhibit the expression of ileal FXR and its downstream targets FGF15 and FGFR4, as well as activate the expression of liver FXR and its downstream target SHP.

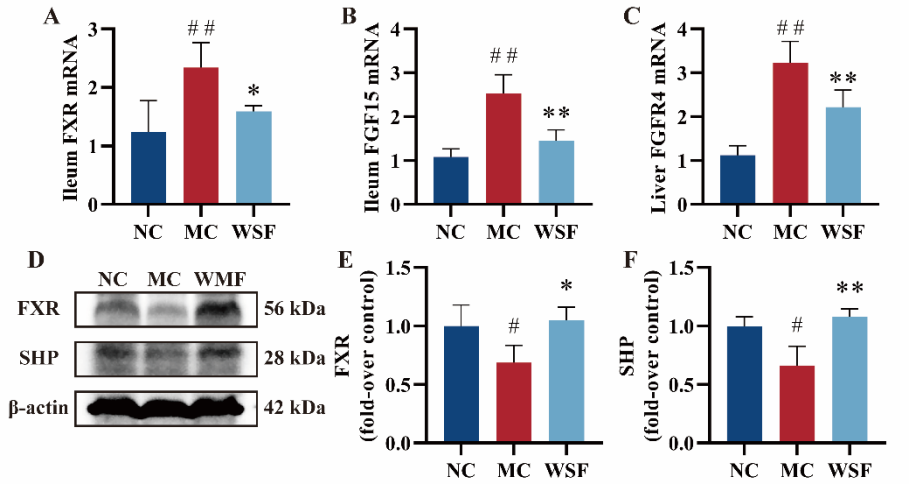

Figure 15 Effects of WSF on the FXR-related pathways in model rats. (A)Ileum *FXR* mRNA. (B) Ileum *FGF15* mRNA. (C) Liver *FGFR4* mRNA. (D) Representative image of liver WB (full-length blots are presented in **Supplementary Figure 3**). (E) Liver FXR. (F) Liver SHP. # ($P < 0.05$), ## ($P < 0.01$) vs. NC; * ($P < 0.05$), ** ($P < 0.01$) vs. MC.

3.10. Effect of WSF on BA transporters

RT-qPCR results indicated that, relative to the NC group, the MC group demonstrated a considerable elevation in ileal *ASBT* mRNA ($P < 0.01$) and a substantial reduction in hepatic *BSEP* mRNA ($P < 0.01$). The W-H group showed a significant inhibition of ileal *ASBT* mRNA expression ($P < 0.01$) and a significant increase in liver *BSEP* mRNA expression ($P < 0.05$) when compared to the MC group (**Figure 16**). These findings suggested that WSF could reduce the reabsorption of BAs in the ileum by inhibiting ileal ASBT and enhance the excretion of BAs from the liver by activating liver BSEP.

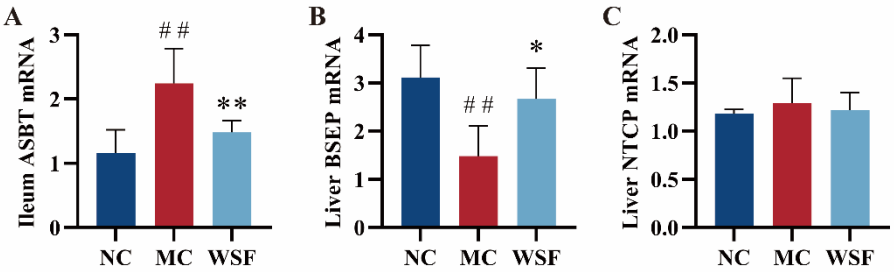

Figure 16 Effects of WSF on BAs transporters in model rats. (A) Ileum *ASBT* mRNA. (B) Liver *BSEP* mRNA. (C) Liver *NTCP* mRNA. # ($P < 0.05$), ## ($P < 0.01$) vs. NC; * ($P < 0.05$), ** ($P < 0.01$) vs. MC.

3.11. Effect of WSF on BA synthase

RT-qPCR results indicated that, compared to the NC group, the MC group showed a significant decrease in liver *CYP27A1* mRNA ($P < 0.05$), with a trend towards a decrease in *CYP7A1* mRNA ($P = 0.101$). The W-H group demonstrated a notable elevation in liver *CYP27A1* mRNA ($P < 0.05$) and a tendency towards increased *CYP7A1* mRNA expression ($P = 0.065$) relative to the MC group (**Figure 17**). These findings indicated that WSF could enhance BA synthesis via the liver's alternative

pathway.

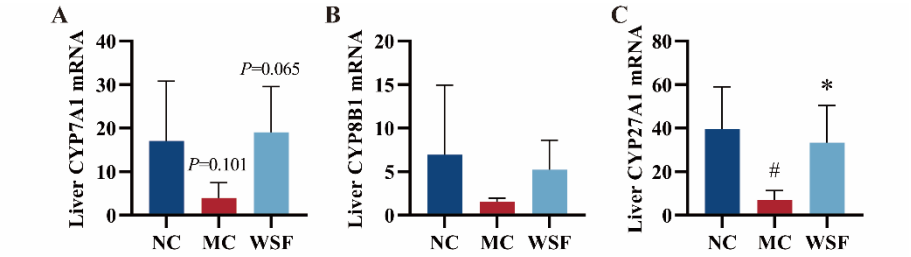

Figure 17 Effects of WSF on BA synthase in the liver of model rats. (A) Liver *CYP7A1* mRNA. (B) Liver *CYP8B1* mRNA. (C) Liver *CYP27A1* mRNA. # ($P < 0.05$), ## ($P < 0.01$) vs. NC; * ($P < 0.05$), ** ($P < 0.01$) vs. MC.

3.12. Effects of WSF on hepatic lipid metabolism

WB results revealed that, compared to the NC group, the MC group showed a considerable increase in the hepatic SCD-1 and SREBP-1c ($P < 0.01$), and a marked decrease in PPAR-α ($P < 0.01$). IF staining results indicated an increase in the expression of liver ACC, SCD-1, SREBP-1c, and SREBP-2 in the MC group.

The WSF group demonstrated a significant reduction in the expression of liver SCD-1 and SREBP-1c ($P < 0.05$; **Figure 18 A, C-D**) and a significant increase in PPAR-α ($P < 0.05$; **Figure 18 A-B**) when compared to the MC group. IF staining results also showed a marked decrease in the expression of liver ACC, SCD-1, SREBP-1c, and SREBP-2 (**Figure 18 E-H**). These findings indicated that WSF could reduce hepatic lipid synthesis and increase lipid β-oxidation in MAFLD model rats.

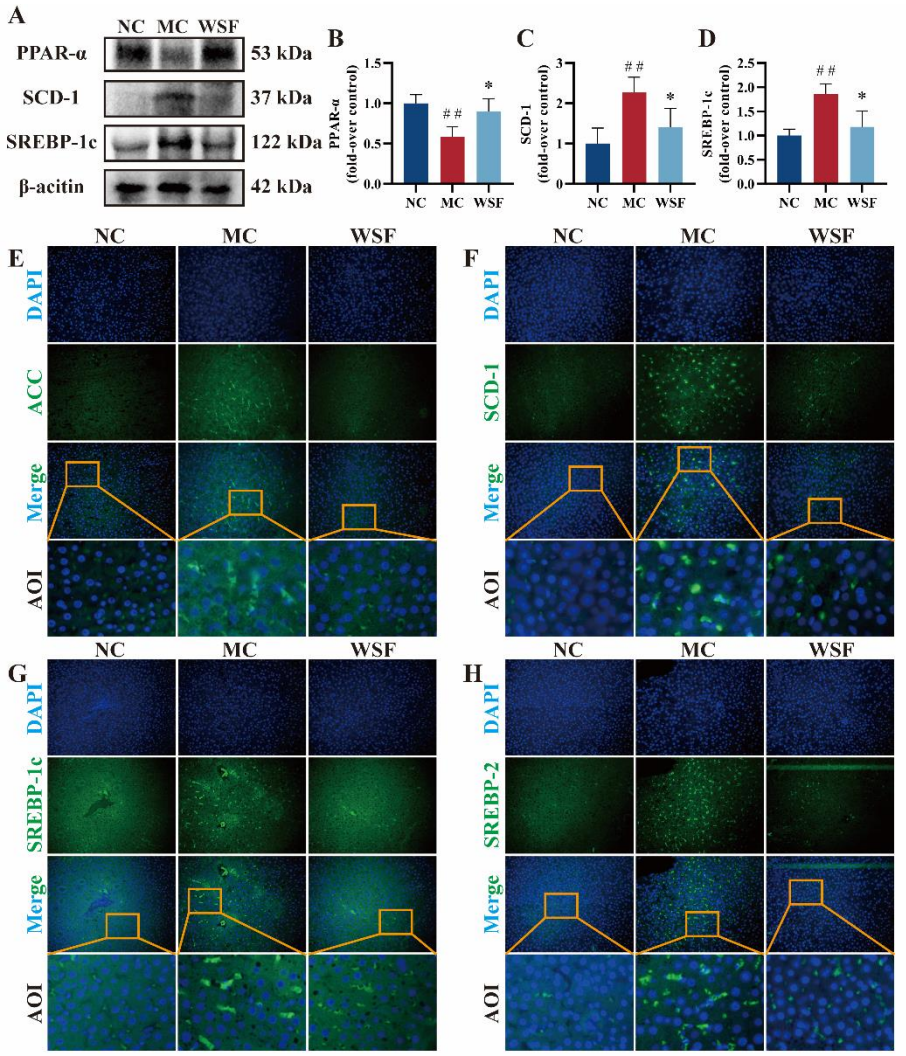

Figure 18 Effects of WSF on the glucolipid metabolic protein in the liver of model rats. (A) Representative image of liver WB (full-length blots are presented in **Supplementary Figure 4**). (B) Liver PPAR-α. (C) Liver SCD-1. (D) Liver SREBP-1c. (E) IF of liver ACC (400×). (F) IF of liver SCD-1 (400×). (G) IF of liver SREBP-1c (400×). (H) IF of liver SREBP-2 (400×). # ($P < 0.05$), ## ($P < 0.01$) vs. NC; * ($P < 0.05$), ** ($P < 0.01$) vs. MC.

4. Discussion

Hundreds of trillions of microorganisms reside in the human gut, performing various biological functions, including modulation of metabolism, inflammation, and maintaining the integrity of the intestinal barrier. Studies have found that obesity-associated gut flora dysbiosis is directly related to excessive dietary fat, characterized by a decrease in total microbial population, lower α diversity, and abnormal changes in species abundance[32, 33]. Saturated fatty acids in the diet can elevate the F/B ratio at the phylum level and diminish the prevalence of probiotics like *Bacteroides*, *Lactobacillus*, and *Bifidobacteria* at the genus level[34-36]. The impact of dietary fats on the gut flora is related to BAs, which act as antimicrobials to disrupt cell membranes and alter the structure of intracellular macromolecules. Consequently, only microbiota capable of tolerating

high levels of BAs can survive in the gut, with unconjugated BAs exhibiting higher antimicrobial activity[37]. In germ-free mice, diet-induced obesity is difficult to achieve. In contrast, obese mice can control their weight through colonization with the gut flora from normal mice, confirming the importance of the gut flora in the development and progression of MAFLD[32]. Our study found altered α diversity indices in the gut flora of MAFLD model rats, with the Ace, Chao, Sobs, and Shannon indices in the W-H group exhibiting similar trends to those in the NC group. Furthermore, β diversity analysis revealed a distinct composition of the gut flora in MAFLD model rats following WSF intervention compared to the MC group.

Certain gut flora can adsorb cholesterol onto cell surfaces, reducing cholesterol absorption. *Lactobacillus gasseri* and *Lactobacillus bulgaricus*, within the *Lactobacillus* genus, secrete peptidoglycans and extracellular polysaccharides that can bind cholesterol to the cell surface[38]. Scholars have isolated the *Lactobacillus gasseri TF08-1* strain from the gut of healthy humans. In vitro and in vivo experiments have demonstrated that this strain could degrade cholesterol, reduce serum TC, TG, LDL-c, and blood viscosity, reverse the abnormal elevation of serum transaminases, and decrease the levels of serum inflammatory factors TNF-α and IL-6[39]. The mechanism by which the *Lactobacillus* genus reduces cholesterol is related to the alteration of the BA pool through BSH. Supplementation with probiotics from the *Lactobacillus* genus can affect the expression of FXR-related pathways, characterized by inhibition of the intestinal FXR-FGF15/19 pathway, activation of the liver FXR-SHP pathway, promotion of liver BA synthesis mediated by enzymes such as CYP7A1 and CYP27A1, and inhibition of intestinal ASBT to reduce BA reabsorption, thereby alleviating liver steatosis[40, 41]. Clinical studies have shown that supplementation with *Lactobacillus* can reduce TC, LDL-c, and non-HDL-c by 4.8%, 8.9%, and 6.0%, respectively, in patients with hypercholesterolemia[42].

BSH is a crucial catalyst for transforming BAs in the intestine and is widely present in the gut flora. However, BSH produced by different bacterial species may have opposite biological effects on the host. *Lactobacillus salivarius*, a member of the *Firmicutes* phylum and the *Lactobacillus* genus, can significantly reduce serum cholesterol and body weight[43]. In contrast, *Bacteroides thetaiotaomicron*, which produces BSH, leads to greater weight gain in mice fed an HFD[44]. It is well known that unconjugated BAs produced by BSH can be further transformed into SBAs, altering the BA profile. BAs can act as signalling molecules to influence the expression of metabolic pathways such as FXR and the G protein-coupled BA receptor 5 (TGR5). The impact on these metabolic pathways depends on the net biological effects of the complex BA profile. Probiotics with BSH activity can down-regulate the expression of intestinal FXR and participate in intestinal cholesterol metabolism. The addition of *Lactobacillus* to the diet down-regulates intestinal FXR expression and promotes the expression of liver CYP7A1, thereby reducing liver cholesterol

levels[45]. Additionally, due to their hydrophobic nature, the free BAs produced by BSH reduce the absorption of dietary lipids and their own reabsorption, increasing the excretion of lipids and BAs in feces[46]. Consistent with the findings above, our study also observed the inhibition of the FXR-FGF15 axis expression in the ileum of MAFLD model rats.

The increased abundance of *Blautia* is associated with obesity and an enlarged BA pool caused by an HFD. Studies have shown that the abundance of potentially harmful species such as *unclassified_g__Blautia* in the gut flora of MAFLD mice significantly increased, and this abundance decreased markedly following pharmacological intervention[47]. Additional studies found that increasing the abundance of *Lactobacillus_johnsonii* could significantly improve the inflammatory response in mice with liver damage and colitis[48, 49]. Furthermore, an elevated abundance of *Lactobacillus_reuteri* has been shown to alleviate chronic constipation in children[50, 51]. Our study also observed similar findings. After 18 weeks of being fed an HSHFD, rats in the MC group experienced a significant increase in the abundance of potentially harmful genera such as *Blautia* and a marked decrease in the abundance of beneficial species like *Lactobacillus*. Moreover, there was a notable rise in the levels of BAs in both serum and liver. After 8 weeks of administration, WSF could modulate the relative abundance of *Lactobacillus*, *Blautia*, and *norank_f__Eubacterium_coprostanoligenes_group* at the genus level in MAFLD model rats and reduce the levels of BAs in serum and liver, with an increase in BAs excretion in feces.

BAs are transformed from cholesterol in the liver, secreted into the intestine, and participate in the digestion and absorption of dietary lipids and lipophilic nutrients[52]. Approximately 95% of BAs in the intestine are reabsorbed in the ileum, while the remainder is excreted in feces. In our study, the levels of BAs in the liver and serum of MAFLD model rats significantly increased, whereas WSF notably reduced the BA pool. The levels of BAs in the liver and serum of MAFLD model rats decreased, and the excretion of BAs in feces significantly increased, indicating that WSF could regulate bile acid metabolism.

Dietary fats stimulate the synthesis and secretion of BAs, which can emulsify fats in the lumen, increase their total surface area, and facilitate their digestion by lipases and absorption by intestinal epithelial cells. There is a direct correlation between fat intake and the synthesis and secretion of BAs[53-55]. In patients with colon cancer on a long-term HSHFD, the levels of SBAs, represented by DCA and LCA, are elevated in feces[56]. The UDCA group can enhance bile secretion and has been used in clinical practice[21]. Compared to conjugated BAs, unconjugated BAs, due to their hydrophobic nature, have a reduced ability to form micelles in the small intestine, thereby decreasing the absorption of dietary lipids. Numerous studies have shown that an increase in BA excretion in feces is positively correlated with liver BA synthesis[57, 58].

BAs are synthesized from cholesterol through two pathways: the classical pathway, involving

enzymes such as CYP7A1 and CYP8B1, which produces CA, and the alternative pathway, involving CYP27A1 and CYP7B1, which synthesizes CDCA. Studies have shown that ileal FXR could regulate the transcription of liver CYP7A1 and CYP27A1, while the expression of CYP8B1 is controlled by liver FXR[59]. Deficiency in BA synthetic enzyme genes can lead to the accumulation of toxic steroid intermediates, resulting in liver injury and cholestasis, which generate toxicity[60].

The activation of the liver FXR-SHP pathway accompanies the detoxification process of BAs. Upon activation, the FXR-SHP axis can enhance BSEP activity, promoting the excretion of BAs from the liver[61]. As one of the primary transporters in the BA cycle, BSEP can only transport BAs conjugated with taurine and glycine and cannot transport unconjugated BAs such as CA and CDCA[62].

Intestinal ASBT is an indispensable component of the BA enterohepatic circulation. Other transporters such as OSTα/β, NTCP, and BSEP can be compensated by MRP1/2/3, OATPs, and MDR2, respectively[63]. FXR regulates the aforementioned BA transporters, with BSEP, MDR3, and OSTα/β being positively regulated by FXR, and NTCP being negatively regulated by FXR[64, 65]. Inhibition of ASBT can reduce the levels of TC and LDL and hinder the progression of liver fibrosis. Clinical trials have also observed a decrease in LDL/HDL in patients with dyslipidemia. The clinical trials of ASBT-targeted inhibitors, *Elobixibat* and *Volixibat*, were ultimately terminated due to their inability to significantly improve ALT levels, liver lipid deposition, and the presence of adverse reactions[66-68]. Targeting a single pathway is often insufficient to achieve a good therapeutic effect on MAFLD. WSF activates BSEP, inhibits ASBT, and improves glycolipid metabolism and liver enzymes in MAFLD model rats. Additionally, its constituent ingredients show no toxicity at the applied doses, demonstrating unique advantages over chemical drugs.

Activation of the liver FXR-SHP pathway can reduce the BA pool and alter the composition of BAs, one of the regulatory pathways being the inhibition of the key enzyme converting cholesterol into BAs[69]. Interestingly, reduced expression of CYP7A1 is often observed in studies on many chronic metabolic diseases, whereas short-term dietary interventions have been associated with increased expression of CYP7A1[70-74]. This may be related to the negative feedback regulation of CYP7A1 by non-FXR-SHP pathways of BAs. Studies have shown that BAs can inhibit the expression of liver CYP7A1 gene by activating intestinal FXR and mediating FGF15-related pathways[70, 75]. Inhibition of intestinal FXR can lead to increased synthesis of liver BAs and increased excretion of BAs in feces[21].

The biological effects induced by FXR activation in the liver and ileum are inconsistent. Liver FXR expression can alleviate liver steatosis and reduce the expression of SREBP-1/2 and the levels of TG and TBA[76, 77]. Clinical studies have also confirmed this viewpoint, with reduced liver FXR expression in patients with MAFLD[17]. Conversely, mice with intestinal-specific FXR knockout exhibit resistance to obesity and reduced liver steatosis after being fed an HFD[78].

The development of FXR agonists or inhibitors has been limited due to the tissue-specific targeting of FXR activation or inhibition. Currently, FDA-approved FXR agonists like obeticholic acid may cause adverse reactions such as itching and deterioration of liver function. The FDA has also issued a black box warning for obeticholic acid, limiting its application. Among the constituent herbs of WSF, *Gynostemmae Herba*, *Astragali Radix*, *Crataegi Fructus*, *Poria*, *Atractylodis Macrocephalae Rhizoma*, and *Citri Reticulatae Pericarpium* are included in the "*Catalog of Substances That Are Both Food and Chinese Herbal Medicine According to Tradition*" published by the State Council of China, highlighting the safety of these herbs[79, 80]. Adverse reaction reports for *Salviae Miltiorrhizae Radix et Rhizoma* have focused on its injectable formulations. The most common adverse reactions were rash and dermatitis[81]. Although there is considerable evidence indicating the safety of the TCM materials in WSF at the applied dosages, the specific safety of WSF still requires validation through systematic toxicological research.

In addition, liver-targeted activation of FXR and intestinal-targeted inhibition can improve BA accumulation by regulating BA transporters and reduce blood lipids and blood glucose by regulating glucose and lipid metabolism, ultimately improving metabolic syndrome. Similar to BAs, the ultimate pharmacological effect of FXR agonists or antagonists is contingent upon the "net effect" of their regulatory influence on the several target genes of FXR.

As endogenous ligands of FXR, BAs activate FXR with varying strengths, with the order being CDCA > DCA = LCA > CA. In rodents, MCA and UDCA, derived from CDCA, act as endogenous inhibitors of FXR. Moreover, most SBAs inhibit FXR. In this study, the liver BA pool in MAFLD model rats decreased, with the reduction in SBAs being approximately twice that of PBAs. The CDCA group increased by 53.8%, leading to an overall effect of activating the expression of FXR-SHP in the liver, thereby activating downstream BSEP expression and inhibiting the expression of SREBP-2, SREBP-1c, and downstream targets SCD-1 and ACC. Due to the regulation of the gut flora by WSF, which affects the metabolism of BAs in the intestine, the expression of ileal FXR-FGF15 was inhibited, relieving the inhibition of liver CYP27A1, promoting liver BA synthesis and

activating FXR in the liver. The activation of FXR in the liver, in turn, inhibited the expression of CYP8B1, resulting in a decrease in CA production in the classical pathway, with an increase in the levels of CDCA and its conjugated forms.

5. Conclusion

In summary, WSF could increase the synthesis of the CDCA group in the liver through the alternative BA synthesis pathway by inhibiting the ileal FXR-FGF15 pathway and promoting the liver FXR-SHP pathway. These promoted liver cholesterol consumption, reduced liver triglyceride synthesis, and increased lipid β-oxidation. However, the specific effects and underlying mechanisms of WSF on MAFLD require further in-depth research.

6. Abbreviations

WSF: Wang's empirical formula; MAFLD: metabolic-dysfunction associated fatty liver; HSHFD: high-sugar and high-fat diet; BA: bile acid; TCM: Traditional Chinese Medicine; PPAR: peroxisome proliferators-activated receptor; SBA: secondary bile acid; ASBT: apical sodium-dependent bile acid transporter; BSH: bile salt hydrolase; DNL: de novo lipogenesis. TBA: total bile acid; FXR: farnesoid X receptor; SHP: small heterodimer partner; BSEP: bile salt export pump; FGF15: fibroblast growth factor 15; FGFR4: fibroblast growth factor receptor 4; GLU: glucose; NEFA: non-esterified fatty acids; IL: interleukin; TNF: tumor necrosis factor; SREBP: sterol regulatory element binding protein; ACC: acetyl-CoA carboxylase; SCD: stearoyl-CoA desaturase; MET: metformin; AUC: area under the curve; FINS: fasting insulin; OGTT: oral glucose tolerance test; PA: perinephric adipose; EA: epididymis adipose; NTCP: sodium taurocholate cotransporting polypeptide.

Declarations

Ethical Statement

Ethics approval number: MGS20231017141. The animal experiments were approved by the Medical Ethics Committee of the Zhejiang University of Technology.

Consent for publication

Not applicable

Data availability statement

The data associated with this study has not been deposited into any publicly available repository. The datasets used and analyzed during the current study are available from the corresponding author upon reasonable request.

Funding

This study was supported by the National Natural Science Foundation of China (No. 81503527 and 82274134), the National Key Research and Development Plan (No. 2017YFC1702200 and 2017YFC1702202), the Key Research and Development Program of Zhejiang Province (No.

2020C04020), and the Science and Technology Department of the State Administration of Traditional Chinese Medicine Zhejiang Province Joint Project (No. GZY-ZJ-KJ-24068).

Authors' contributions

Funding acquisiton & research design: Guiyuan Lv, Suhong Chen, Shuhua Shen, Yihui Zhi, and Kungen Wang. Conducted experiments: Jiahui Huang, Chengliang Zhou, Simei Dong, Yibin Wang, Ning Wang, and Jiujie Jia. Performed data analysis: Jiahui Huang, Chengliang Zhou, Simei Dong, and Chuanjie Zhou; Wrote the manuscript: Suhong Chen, Jiahui Huang, Bo Li, and Xinglishang He. All authors agree to be responsible for all aspects of the work, to ensure completeness and accuracy.

Competing interests

The authors declare that they have no known competing financial interests or personal relationships that could have appeared to influence the work reported in this paper.

References

[1] Younossi, Z.M., Stepanova, M., Afendy, M., et al. Changes in the prevalence of the most common causes of chronic liver diseases in the United States from 1988 to 2008, Clin. Gastroenterol. Hepatol. 9 (2011) 524-530. https://doi.org/10.1016/j.cgh.2011.03.020.

[2] Zhang, L., Ji, G. Expert Consensus on Traditional Chinese Medicine Diagnosis and Treatment of Non-alcoholic Fatty Liver Disease (2023), Chin. J. Integr. Tradit. West. Med. Dig. 32 (2024) 1-7. https://doi.org/10.3969/j.issn.1671-038X.2024.01.01.

[3] Chen, S., Zhou, C., Huang, J., et al. Bioinformatics based exploration of the anti-NAFLD mechanism of Wang's empirical formula via TLR4/NF-κB/COX2 pathway, Mol. Med. 30 (2024) 278. https://doi.org/10.1186/s10020-024-01022-3.

[4] Turnbaugh, P.J., Ridaura, V.K., Faith, J.J., et al. The effect of diet on the human gut microbiome: a metagenomic analysis in humanized gnotobiotic mice, Sci. Transl. Med. 1 (2009) 6-14. https://doi.org/10.1126/scitranslmed.3000322.

[5] Wu, G.D., Chen, J., Hoffmann, C., et al. Linking long-term dietary patterns with gut microbial enterotypes, Science 334 (2011) 105-108. https://doi.org/10.1126/science.1208344.

[6] Moschen, A.R., Kaser, S., Tilg, H. Non-alcoholic steatohepatitis: a microbiota-driven disease, Trends Endocrinol. Metab. 24 (2013) 537-545. https://doi.org/10.1016/j.tem.2013.05.009.

[7] Schnabl, B., Brenner, D.A. Interactions between the intestinal microbiome and liver diseases, Gastroenterology 146 (2014) 1513-1524. https://doi.org/10.1053/j.gastro.2014.01.020.

[8] Yuan, J., Chen, C., Cui, J., et al. Fatty Liver Disease Caused by High-Alcohol-Producing Klebsiella pneumoniae, Cell Metab. 30 (2019) 675-688. https://doi.org/10.1016/j.cmet.2019.08.018.

[9] Archer, R.H., Chong, R., Maddox, I.S. Hydrolysis of bile acid conjugates by Clostridium bifermentans, Euro. J. Appl. Microbiol. Biotech. 14 (1982) 41-45. https://doi.org/10.1007/BF00508002.

[10] Gilliland, S.E., Speck, M.L. Deconjugation of bile acids by intestinal lactobacilli, Appl. Environ. Microbiol. 33 (1977) 15-18. https://doi.org/10.1128/aem.33.1.15-18.1977.

[11] Jones, B.V., Begley, M., Hill, C., et al. Functional and comparative metagenomic analysis of bile salt hydrolase activity in the human gut microbiome, Proc. Natl. Acad. Sci. U. S. A. 105 (2008) 13580-13585. https://doi.org/10.1073/pnas.0804437105.

[12] Ridlon, J.M., Kang, D.J., Hylemon, P.B. Bile salt biotransformations by human intestinal bacteria,

J. Lipid. Res. 47 (2006) 241-259. https://doi.org/10.1194/jlr.R500013-JLR200.
[13] Caligiuri, A., Gentilini, A., Marra, F. Molecular Pathogenesis of NASH, Int. J. Mol. Sci. 17 (2016) 1575. https://doi.org/10.3390/ijms17091575.
[14] Sayin, S.I., Wahlström, A., Felin, J., et al. Gut microbiota regulates bile acid metabolism by reducing the levels of tauro-beta-muricholic acid, a naturally occurring FXR antagonist, Cell Metab. 17 (2013) 225-235. https://doi.org/10.1016/j.cmet.2013.01.003.
[15] Yu, J., Marsh, S., Hu, J., et al. The Pathogenesis of Nonalcoholic Fatty Liver Disease: Interplay between Diet, Gut Microbiota, and Genetic Background, Gastroenterol. Res. Pract. 2016 (2016) 2862173. https://doi.org/10.1155/2016/2862173.
[16] Jiao, N., Baker, S.S., Chapa-Rodriguez, A., et al. Suppressed hepatic bile acid signalling despite elevated production of primary and secondary bile acids in NAFLD, Gut 67 (2018) 1881-1891. https://doi.org/10.1136/gutjnl-2017-314307.
[17] Yang, Z., Shen, W., Sun, H. Effects of nuclear receptor FXR on the regulation of liver lipid metabolism in patients with non-alcoholic fatty liver disease, Hepatol. Int. 4 (2010) 741-748. https://doi.org/10.1007/s12072-010-9202-6.
[18] Lundquist, J.T., Harnish, D.C., Kim, C.Y., et al. Improvement of physiochemical properties of the tetrahydroazepinoindole series of farnesoid X receptor (FXR) agonists: beneficial modulation of lipids in primates, J. Med. Chem. 53 (2010) 1774-1787. https://doi.org/10.1021/jm901650u.
[19] Wahlström, A., Sayin, S.I., Marschall, H.U., et al. Intestinal Crosstalk between Bile Acids and Microbiota and Its Impact on Host Metabolism, Cell Metab. 24 (2016) 41-50. https://doi.org/10.1016/j.cmet.2016.05.005.
[20] Sinal, C.J., Tohkin, M., Miyata, M., et al. Targeted disruption of the nuclear receptor FXR/BAR impairs bile acid and lipid homeostasis, Cell 102 (2000) 731-744. https://doi.org/10.1016/s0092-8674(00)00062-3.
[21] Huang, F., Zheng, X., Ma, X., et al. Theabrownin from Pu-erh tea attenuates hypercholesterolemia via modulation of gut microbiota and bile acid metabolism, Nat. Commun. 10 (2019) 4971. https://doi.org/10.1038/s41467-019-12896-x.
[22] Fang, Y., Hegazy, L., Finck, B.N., et al. Recent Advances in the Medicinal Chemistry of Farnesoid X Receptor, J. Med. Chem. 64 (2021) 17545-17571. https://doi.org/10.1021/acs.jmedchem.1c01017.
[23] Holt, J.A., Luo, G., Billin, A.N., et al. Definition of a novel growth factor-dependent signal cascade for the suppression of bile acid biosynthesis, Genes. Dev. 17 (2003) 1581-1591. https://doi.org/10.1101/gad.1083503.
[24] Kong, B., Wang, L., Chiang, J.Y., et al. Mechanism of tissue-specific farnesoid X receptor in suppressing the expression of genes in bile-acid synthesis in mice, Hepatology. 56 (2012) 1034-1043. https://doi.org/10.1002/hep.25740.
[25] Zhu, Y., Li, F., Guo, G.L. Tissue-specific function of farnesoid X receptor in liver and intestine, Pharmacol. Res. 63 (2011) 259-265. https://doi.org/10.1016/j.phrs.2010.12.018.
[26] Friedewald, W.T., Levy, R.I., Fredrickson, D.S. Estimation of the concentration of low-density lipoprotein cholesterol in plasma, without use of the preparative ultracentrifuge, Clin. Chem. 18 (1972) 499-502.
[27] Chen, S., Huang, J., Huang, Y., et al. Metabolomics analyses reveal the liver-protective mechanism of Wang's metabolic formula on metabolic-associated fatty liver disease, Heliyon 10 (2024) e33418. https://doi.org/10.1016/j.heliyon.2024.e33418.
[28] Lou, X.J., Wang, Y.Z., Lei, S.S., et al. Beneficial Effects of Macroporous Resin Extract of

Dendrobium candidum Leaves in Rats with Hyperuricemia Induced by a High-Purine Diet, Evid.-based Complement. Altern. Med.(2020) 3086106. https://doi.org/10.1155/2020/3086106.
[29] Lei, S., Li, B., Chen, Y., et al. Dendrobii Officinalis, a traditional Chinese edible and officinal plant, accelerates liver recovery by regulating the gut-liver axis in NAFLD mice, J. Funct. Foods 61 (2019) 103458. https://doi.org/https://doi.org/10.1016/j.jff.2019.103458.
[30] Lei, S., Li, B., Chen, Y., et al. Dendrobii Officinalis, a traditional Chinese edible and officinal plant, accelerates liver recovery by regulating the gut-liver axis in NAFLD mice, J. Funct. Foods 61 (2019) 103458. https://doi.org/10.1016/j.jff.2019.103458.
[31] Li, B., He, X., Lei, S.S., et al. Hypertensive Rats Treated Chronically With N(ω)-Nitro-L-Arginine Methyl Ester (L-NAME) Induced Disorder of Hepatic Fatty Acid Metabolism and Intestinal Pathophysiology, Front. Pharmacol. 10 (2019) 1677. https://doi.org/10.3389/fphar.2019.01677.
[32] Bäckhed, F., Ding, H., Wang, T., et al. The gut microbiota as an environmental factor that regulates fat storage, Proc. Natl. Acad. Sci. U. S. A. 101 (2004) 15718-15723. https://doi.org/10.1073/pnas.0407076101.
[33] Ley, R.E., Turnbaugh, P.J., Klein, S., et al. Microbial ecology: human gut microbes associated with obesity, Nature 444 (2006) 1022-1023. https://doi.org/10.1038/4441022a.
[34] Cani, P.D., Bibiloni, R., Knauf, C., et al. Changes in gut microbiota control metabolic endotoxemia-induced inflammation in high-fat diet-induced obesity and diabetes in mice, Diabetes 57 (2008) 1470-1481. https://doi.org/10.2337/db07-1403.
[35] Mokkala, K., Houttu, N., Cansev, T., et al. Interactions of dietary fat with the gut microbiota: Evaluation of mechanisms and metabolic consequences, Clin. Nutr. 39 (2020) 994-1018. https://doi.org/10.1016/j.clnu.2019.05.003.
[36] Murphy, E.F., Cotter, P.D., Healy, S., et al. Composition and energy harvesting capacity of the gut microbiota: relationship to diet, obesity and time in mouse models, Gut 59 (2010) 1635-1642. https://doi.org/10.1136/gut.2010.215665.
[37] Devkota, S., Wang, Y., Musch, M.W., et al. Dietary-fat-induced taurocholic acid promotes pathobiont expansion and colitis in Il10-/- mice, Nature 487 (2012) 104-108. https://doi.org/10.1038/nature11225.
[38] Lye, H., Rahmat-Ali, G.R., Liong, M. Mechanisms of cholesterol removal by lactobacilli under conditions that mimic the human gastrointestinal tract, Int. Dairy J. 20 (2010) 169-175. https://doi.org/https://doi.org/10.1016/j.idairyj.2009.10.003.
[39] Wang, M., Hu, T., Lin, X., et al. Probiotic characteristics of Lactobacillus gasseri TF08-1: A cholesterol-lowering bacterium, isolated from human gut, Enzyme. Microb. Technol. 169 (2023) 110276. https://doi.org/10.1016/j.enzmictec.2023.110276.
[40] Zhang, Z., Zhou, H., Zhou, X., et al. Lactobacillus casei YRL577 ameliorates markers of non-alcoholic fatty liver and alters expression of genes within the intestinal bile acid pathway, Br. J. Nutr. 125 (2021) 521-529. https://doi.org/10.1017/S0007114520003001.
[41] Zhao, M., Kuang, W., Yang, J., et al. Cholesterol lowering in diet-induced hypercholesterolemic mice using Lactobacillus bile salt hydrolases with different substrate specificities, Food Funct. 15 (2024) 1340-1354. https://doi.org/10.1039/d3fo04871c.
[42] Jones, M.L., Martoni, C.J., Prakash, S. Cholesterol lowering and inhibition of sterol absorption by Lactobacillus reuteri NCIMB 30242: a randomized controlled trial, Eur. J. Clin. Nutr. 66 (2012) 1234-1241. https://doi.org/10.1038/ejcn.2012.126.
[43] Joyce, S.A., MacSharry, J., Casey, P.G., et al. Regulation of host weight gain and lipid metabolism

by bacterial bile acid modification in the gut, Proc. Natl. Acad. Sci. U. S. A. 111 (2014) 7421-7426. https://doi.org/10.1073/pnas.1323599111.
[44] Yao, L., Seaton, S.C., Ndousse-Fetter, S., et al. A selective gut bacterial bile salt hydrolase alters host metabolism, Elife 7 (2018) e37182. https://doi.org/10.7554/eLife.37182.
[45] Liang, X., Zhang, Z., Zhou, X., et al. Probiotics improved hyperlipidemia in mice induced by a high cholesterol diet via downregulating FXR, Food Funct. 11 (2020) 9903-9911. https://doi.org/10.1039/d0fo02255a.
[46] Daly, J.W., Keely, S.J., Gahan, C. Functional and Phylogenetic Diversity of BSH and PVA Enzymes, Microorganisms 9 (2021) 732. https://doi.org/10.3390/microorganisms9040732.
[47] Fang, Q., Li, X., Wang, M., et al. Walnut green husk ethanol extract improves gut microbiota and their metabolites associated with NLRP3 in non-alcoholic steatohepatitis, Food Funct. 13 (2022) 6387-6403. https://doi.org/10.1039/d2fo00012a.
[48] Fan, X., Mai, C., Zuo, L., et al. Herbal formula BaWeiBaiDuSan alleviates polymicrobial sepsis-induced liver injury via increasing the gut microbiota Lactobacillus johnsonii and regulating macrophage anti-inflammatory activity in mice, Acta Pharm. Sin. B. 13 (2023) 1164-1179. https://doi.org/10.1016/j.apsb.2022.10.016.
[49] Jia, D., Wang, Q., Hu, Y., et al. Lactobacillus johnsonii alleviates colitis by TLR1/2-STAT3 mediated CD206+ macrophagesIL-10 activation, Gut Microbes 14 (2022) 2145843. https://doi.org/10.1080/19490976.2022.2145843.
[50] Kubota, M., Ito, K., Tomimoto, K., et al. Lactobacillus reuteri DSM 17938 and Magnesium Oxide in Children with Functional Chronic Constipation: A Double-Blind and Randomized Clinical Trial, Nutrients 12 (2020) 225. https://doi.org/10.3390/nu12010225.
[51] Yu, Z., Xiaojia, L., Wei, Z., et al. Baicalin circumvents anti-PD-1 resistance by regulating the gut microbiota metabolite short-chain fatty acids, Pharmacol. Res. 199 (2024) 107033. https://doi.org/10.1016/j.phrs.2023.107033.
[52] Kiriyama, Y., Nochi, H. The Biosynthesis, Signaling, and Neurological Functions of Bile Acids, Biomolecules 9 (2019) 232. https://doi.org/10.3390/biom9060232.
[53] Hill, M.J. Bile, bacteria and bowel cancer, Gut 24 (1983) 871-875. https://doi.org/10.1136/gut.24.10.871.
[54] Reddy, B.S., Mangat, S., Sheinfil, A., et al. Effect of type and amount of dietary fat and 1,2-dimethylhydrazine on biliary bile acids, fecal bile acids, and neutral sterols in rats, Cancer Res. 37 (1977) 2132-2137.
[55] Reddy, B.S. Diet and excretion of bile acids, Cancer Res. 41 (1981) 3766-3768.
[56] Xu, J., Zhan, Q., Fan, Y., et al. Clinical Aspects of Gut Microbiota in Hepatocellular Carcinoma Management, Pathogens 10 (2021) 782. https://doi.org/10.3390/pathogens10070782.
[57] Herrema, H., Meissner, M., van Dijk, T.H., et al. Bile salt sequestration induces hepatic de novo lipogenesis through farnesoid X receptor- and liver X receptor alpha-controlled metabolic pathways in mice, Hepatology. 51 (2010) 806-816. https://doi.org/10.1002/hep.23408.
[58] Out, C., Hageman, J., Bloks, V.W., et al. Liver receptor homolog-1 is critical for adequate up-regulation of Cyp7a1 gene transcription and bile salt synthesis during bile salt sequestration, Hepatology. 53 (2011) 2075-2085. https://doi.org/10.1002/hep.24286.
[59] Sayin, S.I., Wahlström, A., Felin, J., et al. Gut microbiota regulates bile acid metabolism by reducing the levels of tauro-beta-muricholic acid, a naturally occurring FXR antagonist, Cell Metab. 17 (2013) 225-235. https://doi.org/10.1016/j.cmet.2013.01.003.

[60] Jiang, L., Zhao, D., Fan, Y., et al. Transcriptome analysis to assess the cholestatic hepatotoxicity induced by Polygoni Multiflori Radix: Up-regulation of key enzymes of cholesterol and bile acid biosynthesis, J. Proteomics 177 (2018) 40-47. https://doi.org/10.1016/j.jprot.2018.02.014.
[61] Collins, S.L., Stine, J.G., Bisanz, J.E., et al. Bile acids and the gut microbiota: metabolic interactions and impacts on disease, Nat. Rev. Microbiol. 21 (2023) 236-247. https://doi.org/10.1038/s41579-022-00805-x.
[62] Telbisz, Á., Homolya, L. Recent advances in the exploration of the bile salt export pump (BSEP/ABCB11) function, Expert Opin. Ther. Targets 20 (2016) 501-514. https://doi.org/10.1517/14728222.2016.1102889.
[63] Alrefai, W.A., Gill, R.K. Bile acid transporters: structure, function, regulation and pathophysiological implications, Pharm. Res. 24 (2007) 1803-1823. https://doi.org/10.1007/s11095-007-9289-1.
[64] Jiang, L., Zhang, H., Xiao, D., et al. Farnesoid X receptor (FXR): Structures and ligands, Comp. Struct. Biotechnol. J.. 19 (2021) 2148-2159. https://doi.org/10.1016/j.csbj.2021.04.029.
[65] Liu, W., Sun, J., Cao, W., et al. Advances in farnesoid X receptor antagonists and their pharmacological activities, Chin. J. Clin. Pharmacol. Ther. 25 (2020) 764-774. https://doi.org/10.12092/j.issn.1009-2501.2020.07.008.
[66] Newsome, P.N., Palmer, M., Freilich, B., et al. Volixibat in adults with non-alcoholic steatohepatitis: 24-week interim analysis from a randomized, phase II study, J. Hepatol. 73 (2020) 231-240. https://doi.org/10.1016/j.jhep.2020.03.024.
[67] Rudling, M., Camilleri, M., Graffner, H., et al. Specific inhibition of bile acid transport alters plasma lipids and GLP-1, BMC Cardiovasc. Disord. 15 (2015) 75. https://doi.org/10.1186/s12872-015-0070-9.
[68] Simrén, M., Bajor, A., Gillberg, P.G., et al. Randomised clinical trial: The ileal bile acid transporter inhibitor A3309 vs. placebo in patients with chronic idiopathic constipation--a double-blind study, Aliment. Pharmacol. Ther. 34 (2011) 41-50. https://doi.org/10.1111/j.1365-2036.2011.04675.x.
[69] Li, T., Apte, U. Bile Acid Metabolism and Signaling in Cholestasis, Inflammation, and Cancer, Adv Pharmacol 74 (2015) 263-302. https://doi.org/10.1016/bs.apha.2015.04.003.
[70] Davis, R.A., Miyake, J.H., Hui, T.Y., et al. Regulation of cholesterol-7alpha-hydroxylase: BARELy missing a SHP, J. Lipid. Res. 43 (2002) 533-543. https://doi.org/10.1016/S0022-2275(20)31482-6.
[71] Henkel, A.S., Anderson, K.A., Dewey, A.M., et al. A chronic high-cholesterol diet paradoxically suppresses hepatic CYP7A1 expression in FVB/NJ mice, J. Lipid. Res. 52 (2011) 289-298. https://doi.org/10.1194/jlr.M012781.
[72] Kobayashi, M., Harada, T., Takagi, N., et al. Effects of lactic acid-fermented soymilk on lipid metabolism-related gene expression in rat liver, Biosci. Biotechnol. Biochem. 76 (2012) 19-24. https://doi.org/10.1271/bbb.100354.
[73] Yang, T., Wang, Y., Cao, X., et al. Targeting mTOR/YY1 signaling pathway by quercetin through CYP7A1-mediated cholesterol-to-bile acids conversion alleviated type 2 diabetes mellitus induced hepatic lipid accumulation, Phytomedicine 113 (2023) 154703. https://doi.org/10.1016/j.phymed.2023.154703.
[74] Yu, L., Lu, H., Li, R., et al. Effect of Shuangyu Tiaozhi Decoction on SRB1/CYP7A1/FXR Signaling Pathway in Liver of Hypercholesterolemic Rats, Chin. J. Exp. Tradit. Med. Formulae 27 (2021) 47-55. https://doi.org/10.13422/j.cnki.syfjx.20202106.
[75] De Fabiani, E., Mitro, N., Gilardi, F., et al. Coordinated control of cholesterol catabolism to bile acids and of gluconeogenesis via a novel mechanism of transcription regulation linked to the fasted-to-

fed cycle, J. Biol. Chem. 278 (2003) 39124-39132. https://doi.org/10.1074/jbc.M305079200.
[76] Kim, Y.C., Byun, S., Zhang, Y., et al. Liver ChIP-seq analysis in FGF19-treated mice reveals SHP as a global transcriptional partner of SREBP-2, Genome Biol. 16 (2015) 268. https://doi.org/10.1186/s13059-015-0835-6.
[77] Schmitt, J., Kong, B., Stieger, B., et al. Protective effects of farnesoid X receptor (FXR) on hepatic lipid accumulation are mediated by hepatic FXR and independent of intestinal FGF15 signal, Liver Int. 35 (2015) 1133-1144. https://doi.org/10.1111/liv.12456.
[78] Jiang, C., Xie, C., Li, F., et al. Intestinal farnesoid X receptor signaling promotes nonalcoholic fatty liver disease, J. Clin. Invest. 125 (2015) 386-402. https://doi.org/10.1172/JCI76738.
[79] Hao, D., Liu, C. Deepening insights into food and medicine continuum within the context of pharmacophylogeny, Chin. Herb. Med. 15 (2023) 1-2. https://doi.org/10.1016/j.chmed.2022.12.001.
[80] Yao, R., He, C., Xiao, P. 'Food and medicine continuum' in the East and West: Old tradition and current regulation, Chin. Herb. Med. 15 (2023) 6-14. https://doi.org/10.1016/j.chmed.2022.12.002.
[81] Chen, Y., Li, Q., Liu, W., et al. Research progress on pharmacological action, clinical application and side effects of activeingredients of Salvia miltiorrhiza in the treatment of cardiovascular diseases, J. Pharm. Res. (Jinan, China) 42 (2023) 1028-1034. https://doi.org/10.13506/j.cnki.jpr.2023.12.014.

Supplementary Table 1 Bile acid standards

Name	Lot#	Provider	Name	Lot#	Provider
12-KDCA	2874-014A1	Toronto TRC	HDCA	ZZS18080405	Shanghai ZZBIO
12-KLCA	ZZS19026A3	Shanghai ZZBIO	iso-DCA	21B087-A5	Shanghai ZZBIO
3-DDCA	21B090-A5	Shanghai ZZBIO	iso-LCA	ZZS-20-H228-B3	Shanghai ZZBIO
3β-CA	5-JES-41-2	Toronto TRC	LCA	BCBX0612	Merck KGaA
3β-UDCA	14ELZ1361	Toronto TRC	LCA-3-S	IR-15705	Shanghai ZZBIO
7,12-DKLCA	ZZS20132A5	Shanghai ZZBIO	MDCA	ZZS19082709	Shanghai ZZBIO
7-KDCA	ZZS20132A6	Shanghai ZZBIO	NorCA	12THT1441	Toronto TRC
7-KLCA	ZZS19052301	Shanghai ZZBIO	Nor-DCA	2BHW1133	Toronto TRC
ACA	ZZS19013A9	Shanghai ZZBIO	TCA	ZZS19071701	Shanghai ZZBIO
AlloCA	1GAC521	Toronto TRC	TCDCA	ZZS19070311	Shanghai ZZBIO
CA	SLBV8654	Merck KGaA	TDCA	ZZS19082710	Shanghai ZZBIO
CDCA	SLBV2619	Merck KGaA	THCA	ZZS19071010	Shanghai ZZBIO
CDCA-24-Gln	5-NSR-28-1	Toronto TRC	THDCA	ZZS19040403	Shanghai ZZBIO
CDCA-3-Gln	3MJJ1201	Toronto TRC	TLCA	ZZS19032806	Shanghai ZZBIO
DCA	BCBX5907	Merck KGaA	TUDCA	21J081-Z2	Shanghai ZZBIO
DHC	ZZS20120A6	Shanghai ZZBIO	T-α-MCA	ZZS19061807	Shanghai ZZBIO
DHLCA	ZZS20013A4	Shanghai ZZBIO	T-β-MCA	ZZS-20-112-A8	Shanghai ZZBIO
GCA	ZZS19072304	Shanghai ZZBIO	T-ω-MCA	22B249-A2	Shanghai ZZBIO
GCDCA	ZZS19070309	Shanghai ZZBIO	UCA	3MSE661	Toronto TRC
GDCA	ZZS20018A1	Shanghai ZZBIO	UDCA	SLBX3609	Merck KGaA
GHCA	ZZS-20-023-A1	Shanghai ZZBIO	α-MCA	ZZS-20-S003-A5	Shanghai ZZBIO
GLCA	ZZS19052207	Shanghai ZZBIO	β-MCA	21J082-Q1	Shanghai ZZBIO
GUDCA	ZZS19070310	Shanghai ZZBIO	ω-MCA	21J099-S1	Shanghai ZZBIO
HCA	ZZS-20-062-A4	Shanghai ZZBIO			

Supplementary Table 2 Details of the herbal materials in the WSF

Botanical name	Pharmaceutical Name	Chinese name	Voucher NO.	Ratio
Gynostemma pentaphyllum (Thunb.) Makino	*Gynostemmae Herba*	Jiaogulan	230801	10
Hedysarum polybotrys Hand. -Mazz	*Astragali Radix*	Huangqi	230802	10
Crataegus pinnatifida Bge.	*Crataegi Fructus*	Shanzha	230801	4
Salvia miltiorrhiza Bge.	*Salviae Miltiorrhizae Radix et Rhizoma*	Danshen	230601	5
Poria cocos (Schw.) Wolf	*Poria*	Fuling	230201	5
Atractylodes macrocephala Koidz.	*Atractylodis Macrocephalae Rhizoma*	Baizhu	230501	4
Citrus reticulata Blanco	*Citri Reticulatae Pericarpium*	Chenpi	230601	3

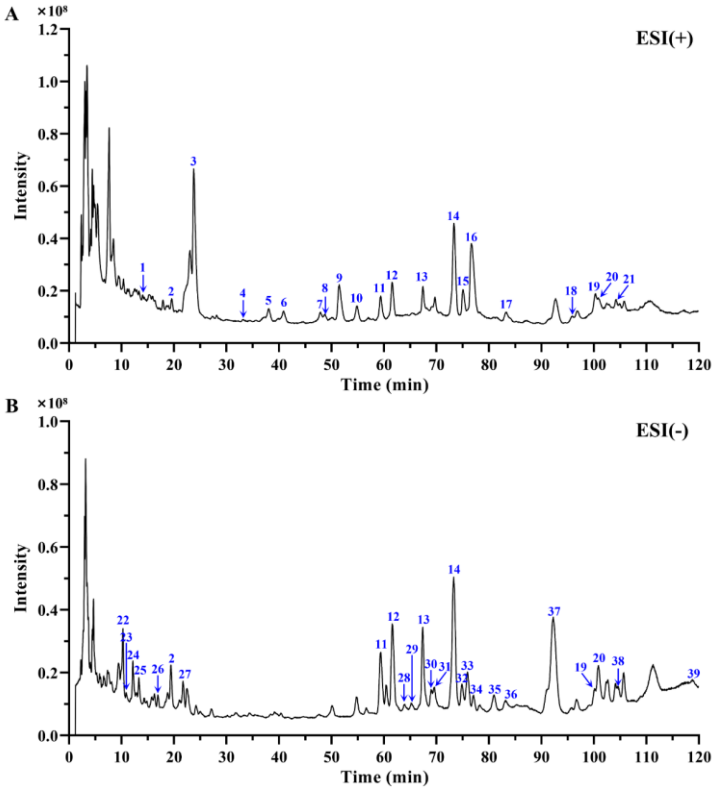

Supplementary Figure 1 The total ion chromatogram (TIC) profiles of WSF[3]. (A) TIC in positive ion mode. (B) TIC in negative ion mode. (C) Peaks 1-39 correlate with the compounds enumerated in **Supplementary Table 3**.

Supplementary Table 3 Identification of chemical compounds in WSF via HPLC-Q-TOF/MS[3]

No.	RT (min)	Putative compounds	Molecular formula	Observed m/z	Theoretical m/z	Error (ppm)	Score	ESI mode	CAS number
1	14.021	Higenamine	$C_{16}H_{17}NO_3$	272.1273	271.1208	3.59	94.64	+	5843-65-2
2	19.589	Chlorogenic acid	$C_{16}H_{18}O_9$	355.1011	354.0951	3.85	91.21	+	327-97-9
	19.404	Chlorogenic acid	$C_{16}H_{18}O_9$	353.0879	354.0951	0.20	97.67	-	327-97-9
3	23.777	Sinapine	$C_{16}H_{24}NO_5$	310.1642	310.1654	2.32	95.86	+	18696-26-9
4	33.151	Phenprobamate	$C_{10}H_{13}NO_2$	180.1008	179.0946	6.05	93.81	+	673-31-4
5	38.053	(-)-Armepavine	$C_{19}H_{23}NO_3$	314.1745	313.1678	2.20	96.73	+	524-20-9
6	40.895	(-)-N-Methylcoclaurine	$C_{18}H_{21}NO_3$	300.1589	299.1521	2.24	95.60	+	5096-70-8
7	47.909	Asimilobine	$C_{17}H_{17}NO_2$	268.1323	267.1259	3.91	93.42	+	6871-21-2
8	48.757	Coclaurine	$C_{17}H_{19}NO_3$	286.1435	285.1365	1.71	97.00	+	486-39-5
9	51.466	N-nornuciferine	$C_{18}H_{19}NO_2$	282.1482	281.1416	2.61	97.28	+	3153-55-7
10	54.823	Calycosin 7-galactoside	$C_{22}H_{22}O_{10}$	447.1280	446.1213	1.77	96.77	+	114272-30-9
11	59.310	Rutin	$C_{27}H_{30}O_{16}$	611.1598	610.1534	2.00	94.97	+	153-18-4
	59.310	Rutin	$C_{27}H_{30}O_{16}$	609.1455	610.1534	1.28	97.92	-	153-18-4
12	61.570	Quercituron	$C_{21}H_{18}O_{13}$	479.0810	478.0747	2.56	95.12	+	22688-79-5
	61.652	Quercituron	$C_{21}H_{18}O_{13}$	477.0671	478.0747	1.09	98.32	-	22688-79-5

13	67.404	Naringin	$C_{27}H_{32}O_{14}$	581.1857	580.1792	1.90	96.19	+	10236-47-2
	67.369	Naringin	$C_{27}H_{32}O_{14}$	579.1712	580.1792	1.57	97.49	-	10236-47-2
14	73.321	Hesperidin	$C_{28}H_{34}O_{15}$	611.1960	610.1898	1.96	96.28	+	520-26-3
	73.269	Hesperidin	$C_{28}H_{34}O_{15}$	609.1818	610.1898	1.48	97.56	-	520-26-3
15	75.082	O-nornuciferine	$C_{18}H_{19}NO_2$	282.1482	281.1416	2.61	97.28	+	3153-55-7
16	76.695	(-)-Nuciferine	$C_{19}H_{21}NO_2$	296.1638	295.1572	3.23	95.11	+	475-83-2
17	83.243	Ononin	$C_{22}H_{22}O_9$	431.1322	430.1264	3.83	89.01	+	486-62-4
18	95.807	Methylnissolin	$C_{17}H_{16}O_5$	301.1055	300.0998	5.57	87.22	+	73340-41-7
19	100.261	Wogonin	$C_{16}H_{12}O_5$	285.0750	284.0685	3.14	95.60	+	632-85-9
	100.110	Wogonin	$C_{16}H_{12}O_5$	283.0613	284.0685	0.26	97.79	-	632-85-9
20	100.943	Quercetin	$C_{15}H_{10}O_7$	303.0492	302.0427	2.89	95.01	+	117-39-5
	100.841	Quercetin	$C_{15}H_{10}O_7$	301.0353	302.0427	0.62	98.27	-	117-39-5
21	104.200	Poncirin	$C_{28}H_{34}O_{14}$	595.2003	594.1949	3.52	88.63	+	14941-08-3
22	10.280	Danshensu	$C_9H_{10}O_5$	197.0457	198.0528	-0.65	98.48	-	42085-50-7
23	10.895	Vanillic acid	$C_8H_8O_4$	167.0351	168.0423	-0.48	98.74	-	121-34-6
24	12.161	Protocatechuic acid	$C_7H_6O_4$	153.0195	154.0266	-0.82	86.79	-	99-50-3
25	13.305	Neochlorogenic acid	$C_{16}H_{18}O_9$	353.0877	354.0951	0.80	97.77	-	906-33-2
26	16.928	Protocatechualdehyde	$C_7H_6O_3$	137.0246	138.0317	-0.73	99.29	-	139-85-5
27	21.731	Cryptochlorogenic acid	$C_{16}H_{18}O_9$	353.0877	354.0951	0.65	97.38	-	905-99-7
28	63.845	Triphasiol	$C_{19}H_{24}O_6$	347.1493	348.1573	2.48	94.09	-	81445-98-9
29	65.241	Carinol	$C_{20}H_{26}O_7$	377.1592	378.1679	4.04	92.22	-	58139-12-1
30	68.998	Azelaic acid	$C_9H_{16}O_4$	187.0977	188.1049	-0.12	98.67	-	123-99-9
31	69.612	Astragalin	$C_{21}H_{20}O_{11}$	447.0921	448.1006	2.55	44.64	-	480-10-4
32	74.831	Paramiltioic acid	$C_{19}H_{24}O_5$	331.1549	332.1624	0.91	98.82	-	140396-85-6
33	75.928	Rosmarinic acid	$C_{18}H_{16}O_8$	359.0774	360.0845	0.19	98.15	-	20283-92-5
34	76.992	Marmin	$C_{19}H_{24}O_5$	331.1551	332.1624	0.55	98.30	-	14957-38-1
35	80.964	Salvianolic acid A	$C_{26}H_{22}O_{10}$	493.1145	494.1213	0.16	96.16	-	96574-01-5
36	84.687	Isorhamnetin	$C_{16}H_{12}O_7$	315.0516	316.0583	-0.84	96.37	-	480-19-3
37	92.215	Salvianolic acid B	$C_{36}H_{30}O_{16}$	717.1455	718.1534	0.99	97.51	-	121521-90-2
38	104.564	Monomethyl lithospermate	$C_{28}H_{24}O_{12}$	551.1190	552.1268	1.69	95.46	-	933054-33-2
39	118.009	Ombuin	$C_{17}H_{14}O_7$	329.0670	330.0740	-0.28	97.70	-	552-54-5

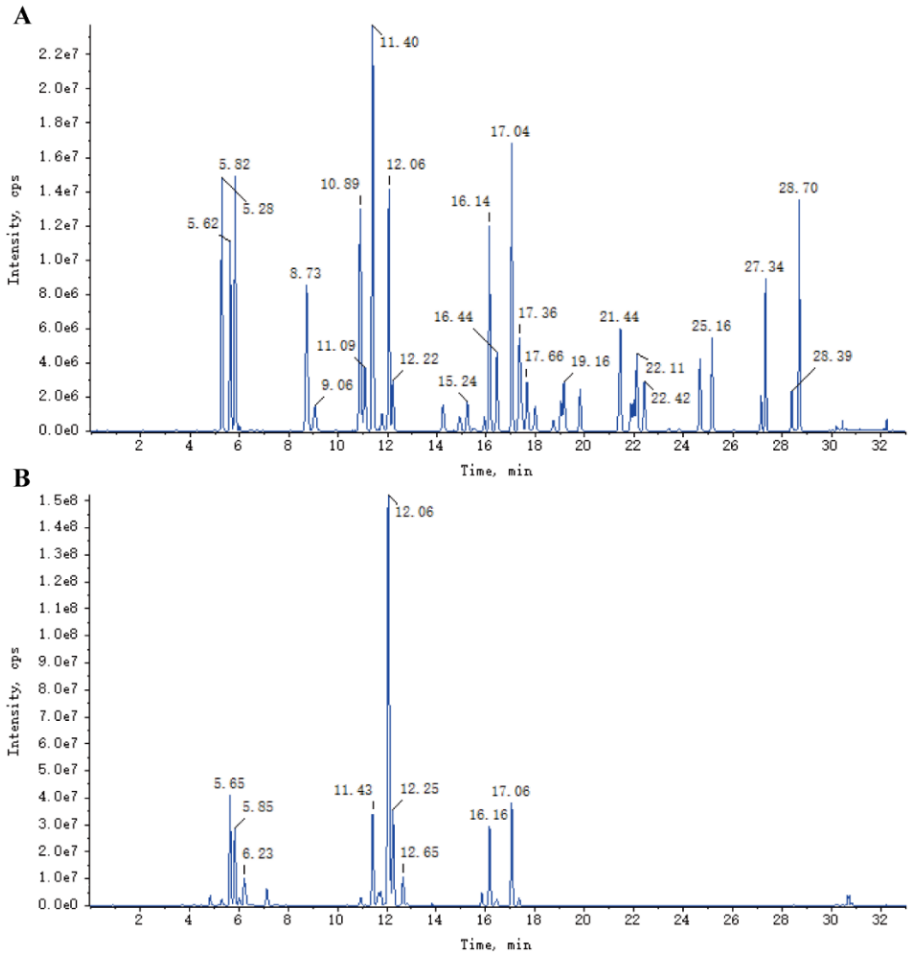

Supplementary Figure 2 TIC of hepatic bile acids. (A) TIC of standards. (B) TIC of liver.

Supplementary Table 4 Linear equations of 47 bile acids

No.	Name	Scale(ng/mL)	Linear equation	R^2
1	GCA	0.20000-1000.00000	y=2.16287x+0.00167	0.9913
2	GCDCA	0.20000-1000.00000	y=2.05997x+0.00237	0.9974
3	TCA	0.20000-1000.00000	y=1.32292x+0.00212	0.9968
4	TCDCA	0.20000-1000.00000	y=3.76215x+0.00274	0.9970
5	GUDCA	0.20000-1000.00000	y=3.90170x+0.00236	0.9968
6	AlloCA	0.50000-500.00000	y=0.84050x-0.00114	0.9913
7	UDCA	0.20000-1000.00000	y=1.34050x+8.43205e-4	0.9953
8	DCA	0.50000-1000.00000	y=0.74472x+0.04230	0.9951
9	TUDCA	0.20000-1000.00000	y=3.53952x+0.00282	0.9965
10	HDCA	0.20000-1000.00000	y=0.75454x+2.32159e-4	0.9954
11	ACA	0.20000-1000.00000	y=0.74097x+4.32264e-5	0.9917
12	GDCA	0.20000-1000.00000	y=4.76075x+0.00332	0.9938
13	GLCA	0.20000-1000.00000	y=2.45381x+5.16128e-4	0.9973
14	α-MCA	1.00000-1000.00000	y=0.55667x-0.00300	0.9967
15	β-MCA	2.00000-1000.00000	y=0.16716x+4.80831e-5	0.9972
16	7-KLCA	0.20000-1000.00000	y=1.31355x+7.52561e-4	0.9918

17	T-α-MCA	0.20000-1000.00000	y=5.15015x-0.00118	0.9971
18	T-β-MCA	0.20000-1000.00000	y=7.05373x-4.81536e-4	0.9936
19	ω-MCA	2.00000-1000.00000	y=0.32830x-4.18848e-4	0.9980
20	MDCA	0.20000-1000.00000	y=0.80040x-2.03632e-4	0.9939
21	THDCA	0.20000-1000.00000	y=13.78247x+0.00340	0.9948
22	THCA	0.20000-1000.00000	y=6.29516x+0.00141	0.9973
23	TLCA	0.20000-1000.00000	y=6.23532x+2.61528e-4	0.9965
24	TDCA	0.20000-1000.00000	y=4.16597x+0.00188	0.9955
25	LCA	0.50000-1000.00000	y=2.25713x+0.12325	0.9930
26	CA	0.20000-1000.00000	y=2.03289x+0.00221	0.9906
27	CDCA	0.50000-1000.00000	y=1.21832x+0.00857	0.9946
28	HCA	0.50000-1000.00000	y=0.90320x-8.22149e-4	0.9944
29	NorCA	0.20000-1000.00000	$y=0.82312x+4.16563e^{-4}$	0.9946
30	GHCA	0.20000-1000.00000	y=1.54067x+0.00124	0.9932
31	Nor-DCA	0.50000-1000.00000	$y=1.31302x+5.08602e^{-5}$	0.9968
32	iso-LCA	0.20000-1000.00000	y=1.06393x+0.01045	0.9935
33	12-KLCA	0.20000-1000.00000	y=1.27674x+0.00173	0.9958
34	DHLCA	0.50000-1000.00000	y=12.84429x+0.11219	0.9962
35	LCA-3-S	0.20000-1000.00000	y=10.80831x+0.00555	0.9973
36	CDCA-3-Gln	0.20000-1000.00000	$y=0.88789x-1.74560e^{-5}$	0.9914
37	3β-UDCA	0.20000-1000.00000	$y=1.63389x+4.41196e^{-4}$	0.9943
38	3-DDCA	0.20000-500.00000	y=1.45990x-0.00158	0.9928
39	CDCA-24-Gln	1.00000-1000.00000	$y=0.15927x+1.44967e^{-4}$	0.9971
40	12-KDCA	1.00000-1000.00000	$y=0.33727x-7.41649e^{-4}$	0.9949
41	7,12-DKLCA	2.00000-1000.00000	$y=0.14959x+1.23960e^{-4}$	0.9957
42	DHC	0.50000-1000.00000	y=0.60740x+0.00241	0.9967
43	UCA	0.20000-1000.00000	$y=0.88771x+6.00366e^{-4}$	0.9953
44	7-KDCA	0.20000-1000.00000	y=1.37447x+0.00163	0.9938
45	iso-DCA	0.20000-1000.00000	y=0.75563x+0.00183	0.9963
46	3β-CA	0.20000-1000.00000	$y=1.15559x+8.20731e^{-4}$	0.9948
47	T-ω-MCA	0.20000-1000.00000	y=6.32914x+0.00126	0.9947

Supplementary Table 5 Stability of bile acids in QC samples

No.	Name	RSD(%)	No.	Name	RSD(%)
1	GCA	10.27	24	TDCA	5.64
2	GCDCA	13.08	25	LCA	6.17
3	TCA	1.34	26	CA	1.49
4	TCDCA	8.75	27	CDCA	3.48
5	GUDCA	3.71	28	HCA	2.82
6	AlloCA	2.96	29	NorCA	9.0
7	UDCA	9.62	30	GHCA	9.05

8	DCA	7.24	31	Nor-DCA	3.33
9	TUDCA	5.53	32	iso-LCA	3.53
10	HDCA	2.19	33	12-KLCA	2.51
11	ACA	4.95	34	DHLCA	2.31
12	GDCA	4.25	35	LCA-3-S	4.76
13	GLCA	9.56	36	CDCA-3-Gln	4.1
14	α-MCA	2.79	37	3β-UDCA	2.75
15	β-MCA	3.56	38	3-DDCA	7.21
16	7-KLCA	1.74	39	CDCA-24-Gln	3.52
17	T-α-MCA	2.33	40	12-KDCA	8.84
18	T-β-MCA	1.32	41	7,12-DKLCA	5.89
19	ω-MCA	5.55	42	DHC	3.57
20	MDCA	4.15	43	UCA	1.68
21	THDCA	2.65	44	7-KDCA	3.55
22	THCA	4.6	45	iso-DCA	8.15

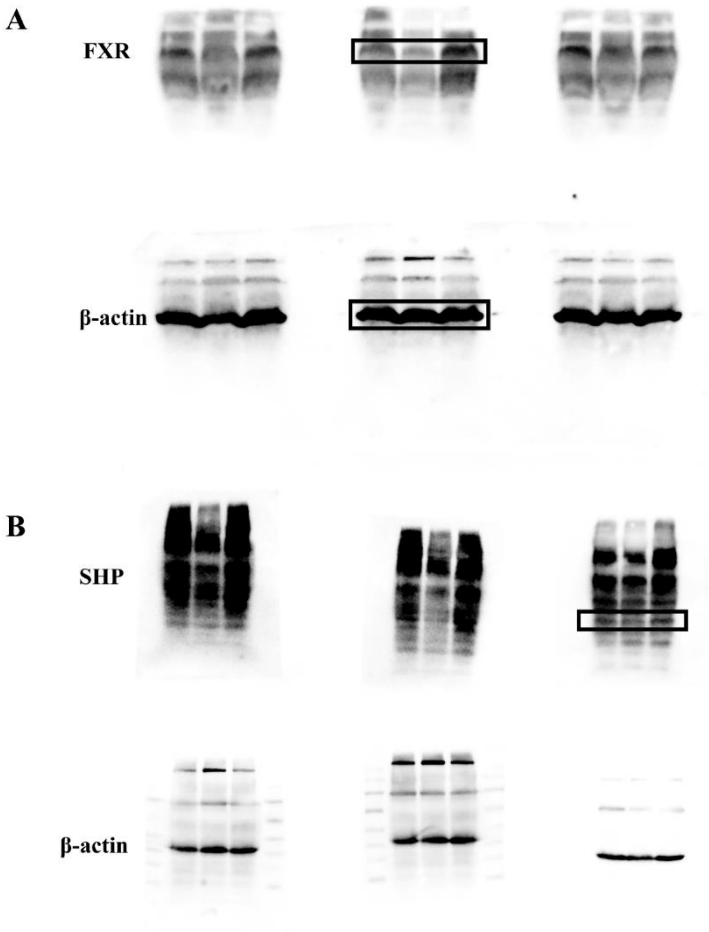

Supplementary Figure 3 Full-length blots in figure 15. (A) FXR and β-actin. (B) SHP and β-actin.

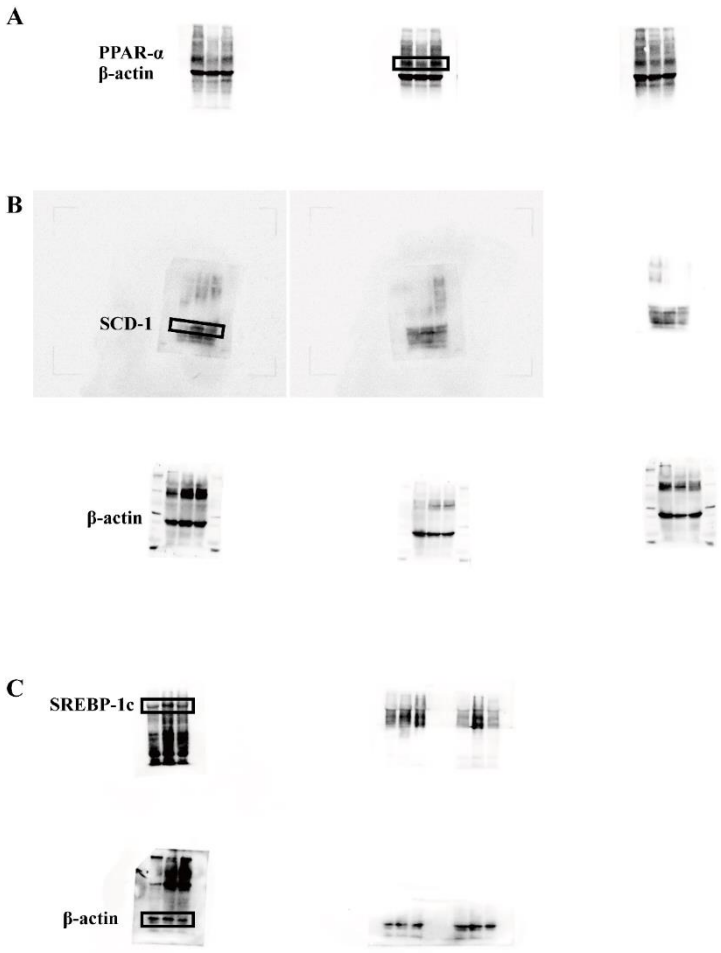

Supplementary Figure 4 Full-length blots in figure 18. (A) PPAR-α and β-actin. (B) SCD-1 and β-actin. (C) SREBP-1c and β-actin.